First Principles Theory of Magneto–Crystalline Anisotropy

O. Eriksson[1] and J. Wills[2]

[1] Department of Physics, Uppsala University, Box 530, S-75112 Uppsala, Sweden
[2] Los Alamos National Laboratory, Los Alamos, NM87545, USA

Abstract. A review of a state of the art, theoretical method for calculating the magneto crystalline anisotropy (MAE) is given. The fundamentals of first principles, total energy calculations, i.e. density functional theory, are described. In addition one of the most common methods for solving the Kohn–Sham equation, the linear muffin–tin orbital method, is described briefly. Technical aspects and difficulties for performing theoretical studies of the MAE are discussed and several examples are given. It is pointed out that the orbital magnetism and the MAE often are intimately connected. The MAE is also argued to be connected to other details of the electronic structure, such as the values of the density of states (DOS) at the Fermi level, the partitioning of the DOS into crystal field components and the hybridization with orbitals of possible ligand atoms.

1 Introduction

Today we are witnessing how modern electronic structure theory has become a very useful theoretical tool in explaining and complementing experiments. Often accurate calculations can reproduce observed magnetic properties such as the occurrence of ferro-, ferri-, antiferro- and paramagnetism. Also, the direction and magnitude of the magnetic moments of bulk, surface and inter-phase systems are normally described well, as is the preferred easy axis of the magnetization direction, something which is called the magneto–crystalline anisotropy-MAE. In addition it has become possible to reproduce the finding that magnetic moments do not always point in the same direction, as is the case in non–collinear magnets and systems with spin spirals [1]. Parallel to this development, theories of micro–magnetism [2] have advanced attempting to describe processes such as magnetization reversal and nucleation when the direction of an external field is changed. These theories describe 'realistic' magnetization phenomena, such as domain formation, domain walls (Bloch and Neel walls), magnetization rotation and curling, etc., which may not always be accessible directly to first principles theorists. However, one important parameter in these theories is the magneto-crystalline anisotropy (MAE). Information of this physical property is often given in terms of the so called anisotropy constants (e.g. K_1 and K_2). Apart from being an important parameter in micro–magnetic models, a deeper insight about the MAE, which shows the directions in the crystal which are easy and hard magnetization directions, is important knowledge in itself. This is not least due to the possibility of designing new materials which are optimal for

H. Dreyssé (Ed.): Workshop 1998, LNP 535, pp. 247–285, 1999.

information storage. Let us illustrate this statement with an example. A small fraction of a magnetic disc with the magnetic moment pointing in one direction may be thought of as representing a 0 in a binary code whereas another section with a reversed moment direction would represent a 1. It becomes important to have the directions well defined, and as a consequence materials with an optimal MAE are searched for. Recently a lot of attention has been focused on orbital magnetism, $\langle L_z \rangle$, of itinerant electron systems, especially since it has been observed that there may be a connection between orbital magnetism and the magneto–crystalline anisotropy (MAE) [3]. As will be argued below, this means that one avenue to find a material with a large MAE is to search for a large orbital moment. At least materials which have a large directional dependence (anisotropy) of the orbital moment are expected to have enhanced MAE [3].

This chapter deals with theoretical aspects of the MAE of transition metals, its relation to important parameters such as the crystal structure, spin and orbital moments, electronic structure and hybridization with possible neighboring atoms. Although several examples of bulk, surfaces and interfaces will be given, this chapter is by far not complete and should not be viewed as an overview of the subject. It is merely intended to illustrate ideas, give understanding and to show ways to think about the MAE. In this chapter we shall thus outline how one can calculate the orbital moment of an itinerant electron system. We also point out that most of the discussion in this chapter deals with elements and compounds where the magnetism is provided by itinerant electrons, electrons which occupy band states that have dispersion (an example of this is bcc Fe). This is in contrast to localized electrons which are atomic like, even in the crystalline environment (an example is hcp Gd, a rare earth element). Calculation of the MAE requires resolving the difference in total energy (which often is of the order of several thousands of Ry) when the magnetization is pointing in two different directions of the solid, with a requirement of accuracy sometimes better than 1 μRy. It is the purpose of this chapter to outline some of the techniques used at present and to give a few examples of the theoretical modeling of magnetism of solids by means of first principles calculations. This chapter begins by reviewing the most important parts of the basis of modern electronic structure theory, namely Density Functional Theory (DFT) [4,5] and the approximations which make it useful for calculations, i.e. the Local Density Approximation (LDA) and the Generalized Gradient Approximation (GGA). The latter two approximations give rise to explicit but approximate expressions of the total energy of a material. At this point we would like to draw attention to the fact that there exist textbooks dealing with this topic; for a more detailed study of DFT, LDA and GGA we refer the reader to Dreitzler and Gross [6], and Eschrig [7]. There are also good review articles on this such as Gunnarsson and Jones [8], and Callaway and March [9]. We will also describe in some detail one of the many methods which exist for calculating the electronic structure and total energy of a solid or a surface, a basis function method based on so–called linear muffin–tin orbitals (LMTO). There are already detailed descriptions of methods for calculating the electronic structure of a solid based on linear muffin–tin or-

bitals [10–12]. However the method outlined here makes fewer approximations and is more accurate. In achieving this there are obstacles which must be overcome which have not been described before, we will try to point these out and compare with the previous methods [10–12]. We would also like to mention that detailed descriptions of other computational methods, such as the Augmented Plane Wave (APW) method of Slater [13] and the modified, linearized version of it (LAPW) by Andersen [10], can be found in Ref. [14] and [15], respectively. Another computational method which calculates the LDA or GGA total energy is based on the so called Linear Combination of Atomic Orbitals (LCAO), orbitals which may be recognized from text books on chemistry and physics of molecules [16]. The LCAO method is described in detail in Refs. [17] and [18] and in addition calculations of the electronic structure of a variety of elements [19] and compounds [20] have been compiled in book form.

2 Introductory Remarks on Electronic Structure Theory

All theories for calculating the magnetic properties and the total energy of solids, surfaces and interfaces start out by adopting the Born–Oppenheimer approximation. This approximation simply neglects the movement of the atomic nuclei and the electrons are considered to be moving around in a material where all nuclei are at fixed positions. The motivation for this is that the electrons are much lighter than the nuclei and thus move much faster. For the materials discussed in this chapter, where the lightest element studied belongs to the 3d series, this approximation is a very good one. One can now focus solely on the electrons, which in itself is a formidable problem. The electrons interact with the positive atomic nuclei and with each other electrons via Coulomb forces. Although the former interaction is by no means simple it can be treated, whereas the latter interaction is impossible to calculate and one must resort to approximations.

Attempts to estimate the electron–electron interaction in solids in order to calculate the electronic dispersion of solids or the total energy of them dates back to the days of the Thomas–Fermi model [21], the Hartree approximation and to the X–α method of Slater [13]. An extension of these ideas culminated in what we today know as Density Functional Theory (DFT) [4,5]. As we will see below this has made it possible to calculate the total energy of for instance a solid, using the electron density, $n(\mathbf{r})$, as the key variable ($n(\mathbf{r})$=$n^{\uparrow}(\mathbf{r})$+$n^{\downarrow}(\mathbf{r})$) where $n^{\uparrow}(\mathbf{r})$ is the spin up electron density and $n^{\downarrow}(\mathbf{r})$ the spin down electron density). For magnetic systems one has also to consider the magnetization density, $m(\mathbf{r})$ ($m(\mathbf{r})$=$n^{\uparrow}(\mathbf{r})$-$n^{\downarrow}(\mathbf{r})$), and examples will be given in this chapter of calculations based on DFT where the total energy and the magnetic properties of a solid are successfully reproduced.

3 Density Functional Theory

3.1 The Hohenberg–Kohn Theorem

Let us start the description of the basic ideas of DFT by considering a non–magnetic system with spin degeneracy[1], the spin polarized case will be discussed later. It is now our purpose to prove the two theorems that are the basis of DFT.

Theorem 1. *The total energy of a system is a unique functional of the ground state electron density.*

To demonstrate this we consider a Hamiltonian, $H = T + V + W$, where T represents the kinetic energy of the system, V the interaction of the electrons with an external potential (normally this is the potential given by the atomic nuclei in the solid) and W the (exact but complex) electron–electron interaction. The solution to this Hamiltonian results in a ground state many body wave function $\Psi(\mathbf{r}_1, \mathbf{r}_2, ...\mathbf{r}_N)$ (for N electrons), and we have

$$H\Psi = E_{\rm gs}\Psi. \tag{1}$$

The electron density can now be calculated from

$$n(\mathbf{r}) = \int d^3r_i \Pi_{i=1}^{N} \mid \Psi(\mathbf{r}_1, \mathbf{r}_2, ...\mathbf{r}_N) \mid^2 \delta(\mathbf{r} - \mathbf{r}_i) \tag{2}$$

and the interaction V is written as $V = \int n(\mathbf{r}) v(\mathbf{r}) d^3r$, where $v(\mathbf{r})$ is the external potential. We will now demonstrate that two different external potentials $v(\mathbf{r})$ and $v'(\mathbf{r})$ must give rise to different ground state electron densities. To show this we note firstly that for the system with potential $v'(\mathbf{r})$ we have

$$H'\Psi' = E'_{\rm gs}\Psi'. \tag{3}$$

From the variational principle it follows that

$$E_{\rm gs} = \langle \Psi \mid H \mid \Psi \rangle < \langle \Psi' \mid H \mid \Psi' \rangle. \tag{4}$$

By adding and subtracting $v'(r)$ on the rhs. of (4) we obtain

$$\begin{aligned} \langle \Psi' \mid H \mid \Psi' \rangle &= \langle \Psi' \mid H' + V - V' \mid \Psi' \rangle \\ &= E'_{\rm gs} + \int n'(\mathbf{r})(v(\mathbf{r}) - v'(\mathbf{r}))d^3r. \end{aligned} \tag{5}$$

Combining the expressions in (4) and (5) gives,

$$E_{\rm gs} < E'_{\rm gs} + \int n'(\mathbf{r})(v(\mathbf{r}) - v'(\mathbf{r}))d^3r. \tag{6}$$

[1] A more elaborate discussion of the contents of this chapter may be found in the text book by Dreitzler and Gross [6].

A similar argument starting from the expression

$$E'_{\rm gs} = \langle \Psi' \mid H' \mid \Psi' \rangle < \langle \Psi \mid H' \mid \Psi \rangle, \tag{7}$$

results in

$$E'_{\rm gs} < E_{\rm gs} + \int n(\mathbf{r})(v'(\mathbf{r}) - v(\mathbf{r}))d^3r. \tag{8}$$

We will now show that if we assume that $n'(\mathbf{r}) = n(\mathbf{r})$ an absurd result emerges and hence this assumption must be wrong, i.e. $n'(\mathbf{r}) \neq n(\mathbf{r})$. The absurdity comes from the fact that if (6) and (8) are added and one assumes $n'(\mathbf{r}) = n(\mathbf{r})$ one obtains the equation

$$E_{\rm gs} + E'_{\rm gs} < E'_{\rm gs} + E_{\rm gs}, \tag{9}$$

which is clearly wrong. Hence $n'(\mathbf{r}) \neq n(\mathbf{r})$ and we conclude that knowledge of the electron density, $n(\mathbf{r})$, implies that we know it was calculated from a Hamiltonian with an external potential $v(\mathbf{r})$ (since we just showed that $v(\mathbf{r})$ and $v'(\mathbf{r})$ give rise to different densities $n(\mathbf{r})$ and $n'(\mathbf{r})$). As the kinetic energy, T, and electron–electron interactions, W, are known and specified we conclude that knowledge of the ground state electron density determines the entire Hamiltonian and hence the ground state energy, which proves Theorem 1 (although an explicit and practical form for calculating $E_{\rm gs}$ from $n(\mathbf{r})$ is not clear from the arguments given above). One can thus express a functional relationship between the ground state energy and the corresponding electron density as

$$E[n(\mathbf{r})] = T[n(\mathbf{r})] + V[n(\mathbf{r})] + W[n(\mathbf{r})]. \tag{10}$$

Since the arguments that lead to this relationship do not depend on the form of $v(\mathbf{r})$ (and hence is valid for atoms, molecules and solids) the kinetic energy and electron–electron interaction $T + W \equiv F[n(\mathbf{r})]$ is called a *universal* functional of the electron density.

A second important theorem of DFT is

Theorem 2. *The exact ground state density minimizes E[n(**r**)].*

This statement partly follows from the fact that the many electron wave function is also specified by the electron density [6], since the ground state density specifies the Hamiltonian and hence also the wave function (of the ground state and of excited states), and to illustrate this dependence we write $\Psi[n(\mathbf{r})]$. To prove Theorem 2 we next note that for a given external potential $v_0(\mathbf{r})$ we can from Theorem 1 write

$$E_{v_0}[n(\mathbf{r})] =< \Psi[n(\mathbf{r})] \mid T + W + V_0 \mid \Psi[n(\mathbf{r})] >, \tag{11}$$

where the subscript v_0 indicates that this is the energy functional for a system with external potential $v_0(\mathbf{r})$. If we now denote the ground state electron density

by $n_0(\mathbf{r})$ we can express the ground state as $\Psi[n_0(\mathbf{r})]$. From the variational principle we again obtain

$$\langle \Psi[n_0(\mathbf{r})] \mid T + W + V_0 \mid \Psi[n_0(\mathbf{r})] \rangle < \langle \Psi[n(\mathbf{r})] \mid T + W + V_0 \mid \Psi[n(\mathbf{r})] \rangle, \tag{12}$$

which can also be expressed as

$$E_{v_0}[n_0(\mathbf{r})] < E_{v_0}[n(\mathbf{r})], \tag{13}$$

i.e., the ground state density minimizes the energy functional $E[n(\mathbf{r})]$, which is what Theorem 2 states. If we now had an explicit form for $E[n(\mathbf{r})]$ we could go ahead and minimize it with respect to the electron density and in this way calculate the ground state energy. Unfortunately one must resort to approximations to obtain an explicit expression for $E[n(\mathbf{r})]$, due to the complexity provided by the electron–electron interactions. We will outline such approximations in the next section but before we do this we note that the arguments above can also be repeated for spin polarized systems and one may show that the ground state energy is a unique functional of the electron and magnetization density. The proof of this is quite similar to the proof outlined above, and we start out by modifying the Hamiltonian to include an external magnetic field, $\mathbf{B}(\mathbf{r})$, so that we have $H = T + W + U$, where $U = \int v(\mathbf{r})n(\mathbf{r}) - \mathbf{B}(\mathbf{r}) \cdot \mathbf{m}(\mathbf{r}) \, \mathrm{d}^3 r$. Based on the variational principle we may, analogous to the discussion around Eqns.4-6, arrive at

$$E_{\mathrm{gs}} < E'_{\mathrm{gs}} + \int n'(\mathbf{r})(v(\mathbf{r}) - v'(\mathbf{r}))d^3r - \int \mathbf{m}'(\mathbf{r})(\mathbf{B}(\mathbf{r}) - \mathbf{B}'(\mathbf{r}))d^3r \tag{14}$$

and

$$E'_{\mathrm{gs}} < E_{\mathrm{gs}} + \int n(\mathbf{r})(v'(\mathbf{r}) - v(\mathbf{r}))d^3r - \int \mathbf{m}(\mathbf{r})(\mathbf{B}'(\mathbf{r}) - \mathbf{B}(\mathbf{r}))d^3r. \tag{15}$$

If we again assume that $n(\mathbf{r}) = n'(\mathbf{r})$ and $\mathbf{m}(\mathbf{r}) = \mathbf{m}'(\mathbf{r})$ and add (14) and (15) we arrive at the same absurd result as in the discussion of spin degenerate systems, i.e. (9), and we must draw the conclusion that $n(\mathbf{r}) \neq n'(\mathbf{r})$ and $\mathbf{m}(\mathbf{r}) \neq \mathbf{m}'(\mathbf{r})$. Hence we may conclude that for magnetic systems we can write the ground state energy as a unique functional of the electron density and the magnetization density.

3.2 The Kohn–Sham Approach

The theorems described above are also valid for non–interacting electron systems where the part of the Hamiltonian describing electron–electron interactions, W, is absent. In this case electrons which move in the field of an external potential which, we for reasons that will be obvious below, call V_{eff}, are solutions to a one–electron Schrödinger equation,

$$[\frac{-\nabla^2}{2} + V_{\mathrm{eff}}]\psi_i = E_i\psi_i. \tag{16}$$

There is an infinity of solutions to this equation and to specify a special solution the subscript i is introduced. From (16) one can calculate an electron density from the lowest lying one–particle (op) states. If there are N electron states which are solutions to (16) one simply calculates the one-particle (a label introduced to show that there are no electron–electron interactions considered) electron density from

$$n_{\rm op}(\mathbf{r}) = \sum_{i=1}^{N/2} 2 \mid \psi_i(\mathbf{r}) \mid^2, \tag{17}$$

where the factor 2 comes from spin degeneracy. In this case the energy functional which describes the total energy of the N electrons may be written as,

$$E_{\rm op}[n_{\rm op}(\mathbf{r})] \equiv T_{\rm op}[n_{\rm op}] + V_{\rm eff}[n_{\rm op}] \equiv \sum_{i=1}^{N/2} \langle \psi_i(\mathbf{r}) \mid \frac{-\nabla^2}{2} \mid \psi_i(\mathbf{r}) \rangle + \int n_{\rm op}(\mathbf{r}) V_{\rm eff}(\mathbf{r}) d^3r, \tag{18}$$

and the electron density which minimizes this functional is obtained from the requirement that the energy functional is stationary for small variations of the electron density around the ground state density. This can be written as,

$$0 = \delta E_{\rm op} = E_{\rm op}[n_{\rm op}(\mathbf{r}) + \delta n_{\rm op}(\mathbf{r})] - E_{\rm op}[n_{\rm op}(\mathbf{r})], \tag{19}$$

which may also be written as

$$0 = \delta T_{\rm op}[n_{\rm op}] + \int \delta n(\mathbf{r}) V_{\rm eff}(\mathbf{r}) d^3r. \tag{20}$$

Carrying out the minimization in (20) leads to (16), and we have demonstrated that independent particles which are the solution to (16) give rise to a density which minimizes the total energy expression of independent particles in (18).The reason for introducing (16) to (20) is mainly that they can be solved, at least approximately, to within a desired accuracy (this is the topic of the next subsection), but at this state it is unclear if equations (16) to (20) have anything to do with a 'real' interacting system. However, as will be clear in a moment they can, via the Kohn–Sham approach, be used to actually calculate the ground state energy of a 'real' electron system. The basic principle of the Kohn–Sham approach is now to assume that one can find an effective potential, $V_{\rm eff}$, so that $n_{\rm op}(\mathbf{r})$=$n(\mathbf{r})$, where $n(\mathbf{r})$ is the electron density of the fully interacting ('real') system. Since we know that the total energy of a system is uniquely determined by the electron density it seems to be an efficient route to obtain the correct electron density from a one–electron like problem, in our ultimate quest of calculating the ground state energy of a solid.

The question now is how to determine $V_{\rm eff}$, so that $n_{\rm op}(\mathbf{r})$ becomes equal to $n(\mathbf{r})$. To do this we recast the energy functional in (10) as

$$E[n(\mathbf{r})] = T_{\rm op}[n(\mathbf{r})] + \int n(\mathbf{r})v(\mathbf{r})d^3r + \frac{1}{2}\int\int {\rm e}^2 \frac{n(\mathbf{r})\cdot n(\mathbf{r}')}{\mid \mathbf{r}-\mathbf{r}' \mid} d^3r d^3r' + E_{\rm xc}[n(\mathbf{r})]. \tag{21}$$

Since we require that $n_{\rm op}(\mathbf{r})$ should be equal to $n(\mathbf{r})$ we have in the expression above, for simplicity, skipped the subscript op on the electron density of the right hand side. In (21) we have introduced the one–particle kinetic energy functional instead of the true kinetic energy functional of (10) and we have introduced the Hartree electrostatic interaction instead of the true electron–electron interaction. Hence in order to make (21) equal to (10) we must introduce a term that corrects for these replacements, and this is what the exchange and correlation energy, $E_{\rm xc}[n(\mathbf{r})]$, does. Since the first three terms on the right hand side of (21) are possible to calculate numerically we have moved the complexity of the fully interacting system to finding the exchange and correlation functional. So far it has been impossible to find the exact exchange and correlation functional so that (21) holds for all densities and all systems. However, for a uniform electron gas one can calculate $E_{\rm xc}[n(\mathbf{r})]$[2] for all values of the electron density and parameterized forms of $E_{\rm xc}[n(\mathbf{r})]$ as a function of $n(\mathbf{r})$ is available. The local density approximation assumes that these parameterizations work even in cases where the electron gas is not uniform, but varies is space, as it does in a solid, surface or interface. The local density approximation introduces the following expression for the exchange-correlation energy [6],

$$E_{\rm xc}[n(\mathbf{r})] = \int \epsilon_{\rm xc}[n(\mathbf{r})]n(\mathbf{r})d^3r, \tag{22}$$

where $\epsilon_{\rm xc}[n(\mathbf{r})]$ is named the exchange–correlation energy density and in a parameterized form its dependence on $n(\mathbf{r})$ is relatively simple and may, for example, be found in Ref. [6]. We are now armed with an (approximate) expression for the ground state energy functional and in analogy with (19) and (20) we determine the ground state density from this functional by requiring that the functional (equation (21)) is stationary for small variations of the electron density around the ground state density. By doing this we obtain an expression which is quite similar to (20), i.e. we obtain

$$0 = \delta T_{\rm op}[n] + \int \delta n(\mathbf{r})[v(\mathbf{r}) + \int {\rm e}^2 \frac{n(\mathbf{r}')}{\mid \mathbf{r}-\mathbf{r}' \mid} d^3r' + \frac{\partial(\epsilon_{\rm xc}[n(\mathbf{r})]n(\mathbf{r}))}{\partial n(\mathbf{r})}]. \tag{23}$$

[2] This can be done in the high electron density limit [22] and in the low electron density limit [23]. Interpolation between these two limits gave rise to parameterized forms of the exchange and correlation functional of a uniform electron gas for all values of the density [23]. However, this interpolation is in modern electronic structure calculations replaced by approaches which are based on quantum Monte–Carlo simulations for the intermediate values of the electron gas [24].

We have now achieved our goal in finding the effective potential which (within the approximations and assumptions introduced) ensures that $n_{\rm op}(\mathbf{r})$=$n(\mathbf{r})$, since when we compare (20) and (23) we can identify $V_{\rm eff}$ as,

$$V_{\rm eff}(\mathbf{r}) = v(\mathbf{r}) + \int {\rm e}^2 \frac{n(\mathbf{r}')}{\mid \mathbf{r} - \mathbf{r}' \mid} d^3r' + \mu_{\rm xc}(n(\mathbf{r})), \tag{24}$$

where

$$\mu_{\rm xc}(n(\mathbf{r})) = \frac{\partial(\epsilon_{\rm xc}[n(\mathbf{r})]n(\mathbf{r}))}{\partial n(\mathbf{r})} = \epsilon_{\rm xc}[n(\mathbf{r})] + n(\mathbf{r})\frac{\partial(\epsilon_{\rm xc}[n(\mathbf{r})])}{\partial n(\mathbf{r})}. \tag{25}$$

All we have to do now is to solve (16) with the effective potential specified by (24). Since the effective potential to be used in (16) depends on the electron density, the property we want to calculate, one has to perform a self–consistent field calculation (SCF) where an initial electron density is more or less guessed and an effective potential is calculated from (24). This potential is then used to solve (16) and a new electron density is calculated from (17), which is then put back into (24). This procedure is repeated until convergence is obtained, i.e. until the density does not change appreciably with successive iterations[3]. Once a self–consistent electron density has been found one can calculate the ground state energy of the Kohn–Sham (LDA) energy functional (via (21)) and hence one of the main goals in electronic structure calculations has been achieved.

Before entering the details of how one might solve the self consistent Kohn–Sham equations, (16) and (17), we note that the entire procedure outlined above can also be made to work for magnetic systems. At the end of the previous section we concluded that for magnetic systems the ground state energy may be written as a unique functional of the electron density and of the magnetization density. An alternative way of expressing this is to state that there is an energy functional which depends both on the majority and the minority spin density (since $n(\mathbf{r}) = n^{\uparrow}(\mathbf{r}) + n^{\downarrow}(\mathbf{r})$ and $m(\mathbf{r}) = n^{\uparrow}(\mathbf{r}) - n^{\downarrow}(\mathbf{r})$[4]) and we can write $E[n^{\uparrow}(\mathbf{r}), n^{\downarrow}(\mathbf{r})]$. We can then make an analogous assumption to the discussion around (21) and obtain a Kohn–Sham scheme for spin polarized systems via,

$$E[n^{\uparrow}(\mathbf{r}), n^{\downarrow}(\mathbf{r})] = T_{\rm op}[n^{\uparrow}(\mathbf{r}), n^{\downarrow}(\mathbf{r})] + \int n(\mathbf{r})v(\mathbf{r})d^3r + \frac{1}{2}\int\int {\rm e}^2 \frac{n(\mathbf{r})\cdot n(\mathbf{r}')}{\mid \mathbf{r} - \mathbf{r}' \mid} d^3r d^3r' + E_{\rm xc}[n^{\uparrow}(\mathbf{r}), n^{\downarrow}(\mathbf{r})]. \tag{26}$$

[3] Normally one is forced to mix the electron density which is the output of (17) with the electron density which is in input for that particular loop in the SCF iterational procedure before one takes this *mixed* density and puts it in (24). The whole procedure of *mixing* is quite complex where many suggestions of how to achieve self consistency with as few iterations as possible have been suggested [25].

[4] We note here that this approach has simplified the situation somewhat since the magnetization density is a scalar property with both magnitude and spin. In this analysis we are assuming that the magnetization is pointing only in one direction, the z–direction, of the system.

In a real solid the preference for occupying one spin channel (to some degree) more than the other is traditionally explained as due to the exchange interaction and the driving force for it is the electron–electron interaction in the Hamiltonian. Hence in the spin polarized Kohn–Sham scheme this necessarily means that the exchange and correlation potential, which is supposed to absorb all complex electron–electron interactions, must depend both on the charge and the spin (magnetization) density. Turning again to studies on the uniform electron density is useful and parameterizations for $E_{\rm xc}[n^{\uparrow}(\mathbf{r}), n^{\downarrow}(\mathbf{r})]$, as a function of $n^{\uparrow}(\mathbf{r})$ and $n^{\downarrow}(\mathbf{r})$, have been made. We can now proceed quite analogously to the discussion around (16) and (17) and analyze a one particle Hamiltonian with spin up (down) effective potentials,

$$[\frac{-\nabla^2}{2} + V_{\rm eff}^{\uparrow(\downarrow)}]\psi_i^{\uparrow(\downarrow)} = E_i^{\uparrow(\downarrow)}\psi_i^{\uparrow(\downarrow)}, \tag{27}$$

where the electron density for electrons with a given spin is obtained from,

$$n_{\rm op}^{\uparrow(\downarrow)}(\mathbf{r}) = \sum_{i=1} \mid \psi_i^{\uparrow(\downarrow)}(\mathbf{r}) \mid^2 . \tag{28}$$

Repeating the discussion which led to (24), with the only modification that we now require the energy functional to be stationary with regard to both the spin up and the spin down density, leads to effective potentials which are different for the two spin directions due to differences in the exchange and correlation potential,

$$V_{\rm eff}^{\uparrow(\downarrow)}(\mathbf{r}) = v(\mathbf{r}) + \int {\rm e}^2 \frac{n(\mathbf{r'})}{\mid \mathbf{r} - \mathbf{r'} \mid} d^3r' + \mu_{\rm xc}(n^{\uparrow}(\mathbf{r}), n^{\downarrow}(\mathbf{r})). \tag{29}$$

Hence the simplest forms[5]of spin polarized calculations treat the spin up and spin down electrons separately and for every iteration in the self–consistent loop one solves a Kohn–Sham equation for both spin directions. The spin up and spin down densities are then calculated by occupying the N lowest (spin up or spin down) eigenvalues of the separate two Kohn–Sham equations. Since for a given $V_{\rm eff}^{\uparrow}(\mathbf{r})$ which may be different from $V_{\rm eff}^{\downarrow}(\mathbf{r})$ there may be more spin up states, $E_i^{\uparrow}$ than spin down states, $E_i^{\downarrow}$, which have an energy lower than the highest occupied state (the Fermi level-$E_{\rm F}$) it is clear how spin polarization might occur. With a self consistent spin and magnetization density the magnetic moment is calculated as $\int m(\mathbf{r})d^3r$ (in Bohr magneton units) and the total energy may be calculated from (26).

4 Solving the Kohn–Sham Equations: Bulk

We have shown in the previous subsection that the equations to be solved for calculating the magnetic properties of a solid from first principles are (27)–(29). Before entering the details of one of the most used methods, the Linear

[5] We will discuss below, in connection to the section about orbital moments and relativity, complications which makes this scheme somewhat more involved.

Muffin–Tin Orbital (LMTO) method, we note that due to the symmetry of bulk materials a number of simplifications evolve. This discussion can also be found in, for instance, the textbook by Ashcroft and Mermin [26].

First of all one normally assumes in a bulk material that the potential which enters (27) is periodic, i.e. $V_{\rm eff}^{\uparrow(\downarrow)}(\mathbf{r}) = V_{\rm eff}^{\uparrow(\downarrow)}(\mathbf{r}+\mathbf{R})$, where $\mathbf{R}$ is a translation vector (a Bravais lattice vector) of the solid. This periodic boundary condition leads to Bloch's theorem [26] which states that as an effect of the periodicity of the bulk material the one–electron wave function must obey the following condition,

$$\psi_{i,\mathbf{k}}^{\uparrow(\downarrow)}(\mathbf{r}+\mathbf{R}) = \mathrm{e}^{\mathrm{i}\mathbf{k}\cdot\mathbf{R}}\psi_{i,\mathbf{k}}^{\uparrow(\downarrow)}(\mathbf{r}), \tag{30}$$

and we note that a vector $\mathbf{k}$ has been introduced. This is a vector of reciprocal space[6] and due to the translation symmetry one has only to consider $\mathbf{k}$–vectors which lie inside the first Brillouin zone when looking for solutions to (27)–(29) [26]. In addition one can solve the (27)–(29) for each $\mathbf{k}$–vector being separate and independent of the others. However, the dependence of the one–electron wave function on $\mathbf{k}$ makes the calculation of the one–electron density somewhat more complex since we have to include a sum over all possible $\mathbf{k}$–vectors, and (28) is in a crystal replaced by

$$n_{\rm op}^{\uparrow(\downarrow)}(\mathbf{r}) = \sum_i \sum_{\mathbf{k}} \mid \psi_{i,\mathbf{k}}^{\uparrow(\downarrow)}(\mathbf{r}) \mid^2 . \tag{31}$$

In a similar way one often needs to sum all the possible Kohn–Sham eigenvalues E_i (equation (16)) to be used for calculating the total energy, (26). This is needed since one often writes, $T_{\rm op} = E_{\rm sum} - \int v_{\rm eff}(\mathbf{r})n(\mathbf{r})d^3r)$. The sum of the eigenvalues, $E_{\rm sum}$, is often referred to as the eigenvalue sum and it is calculated from

$$E_{\rm sum} = \sum_i \sum_{\mathbf{k}} E_{i,\mathbf{k}}. \tag{32}$$

In principle all $\mathbf{k}$–vectors inside the first Brillouin zone should be considered in the sums above, but since this number is enormous one would like to replace the sum with an integral. However, if one does not have an analytic dependence of, for instance, E_i of $\mathbf{k}$**,** we must find ways to approximate (32). In order to do this it is useful to introduce the concept of density of states, DOS. A derivation of the DOS may be found in most textbooks on solid state physics and it is not repeated here. Instead we quote the result, that the DOS can be calculated from,

$$D(E) = \sum_i \frac{1}{8\pi^3} \int_{BZ} \delta(E - E_{i\mathbf{k}}) d^3k. \tag{33}$$

[6] Reciprocal space is spanned by the vectors $\mathbf{G}_i$, defined as $\mathbf{G}_i \cdot \mathbf{R}_j = 2\pi\delta_{ij}$, where V is the volume of the primitive cell of the Bravais lattice.

With this definition of the DOS one can calculate the eigenvalue sum from

$$E_{\rm sum} = \int_{-\infty}^{E_{\rm F}} ED(E)dE. \tag{34}$$

4.1 Different Types of k-Space Integration

Having defined the DOS in (33) and the eigenvalue sum, in (34) we are now ready to discuss different ways to approximate the integral over the Brillouin zone (BZ), which is necessary in numerical methods where one does not have an analytical expression of $E_{i\mathbf{k}}$. First we write the eigenvalue sum as,

$$E_{\rm sum} = \sum_i \int_{-\infty}^{\infty} Ef(E)\frac{1}{8\pi^3}\int_{BZ}\delta(E - E_{i\mathbf{k}})d^3kdE, \tag{35}$$

where $f(E)$ is a step function which attains the value one below the Fermi energy and zero above. $E_{\rm sum}$ is numerically very sensitive to the **k**–point sampling and the choice of numerical method to perform the Brillouin–zone integration, BZI. We will discuss three different BZI schemes [27]. In all three cases a uniform mesh of **k**–points is used, distributed as to fulfill the symmetry of the space–group. The BZI can in all three cases be written as weighted sums over the bands, i, and the discrete set of sampled **k**–points, k_j, with weight functions, w_{ji}. In the so–called linear tetrahedron method [28], LTM, the uniform mesh is divided into corner–sharing tetrahedra. A linear interpolation of the eigenvalues is performed between the **k**–points belonging to one tetrahedron, resulting in a weight function w_{ji}. The step function is used directly by using $E_{\rm F}$ as an upper limit in the energy integration. A modification of the linear tetrahedron method, MTM, was suggested by Blöchl et al. [29] In the MTM the linear weights, w_{ji}, are corrected by, $dw_{ij}{=}\sum_T \frac{1}{40}D_T(E_{\rm F})\sum_l^4(E_{il}-E_{ij})$, where T is an index for the tetrahedra and l is an index for the **k**–points at the corners of the tetrahedron T. $D_T(\mathrm{E_F})$ is the contribution to the density of states from the tetrahedron T at the Fermi level and E_{ij} is the i^{th} eigenvalue of the j^{th} **k**-point belonging to the tetrahedron T. The MTM corrects for the curvature of the energy band to leading order. Another way to perform the BZI is to use a Gaussian broadening method, GBM, which convolute each discrete eigenvalue with a Gaussian function of width W. This method and the related Fermi-Dirac broadening method are very popular in total energy methods since they lead to a fast and stable convergence of the charge and spin densities. The GBM can be seen as a truncation of a complete series expansion of a δ–function in terms of Hermite polynomials, H_n, with a Gaussian weight function [30]. Then the step function, $f(E)$, can be written as

$$f(E) = f_0(E,W) + \sum_{n=1}^{\infty} A_n H_{2n-1}\left(\frac{E-E_{\rm F}}{W}\right)\mathrm{e}^{-\left(\frac{E-E_{\rm F}}{W}\right)^2}, \tag{36}$$

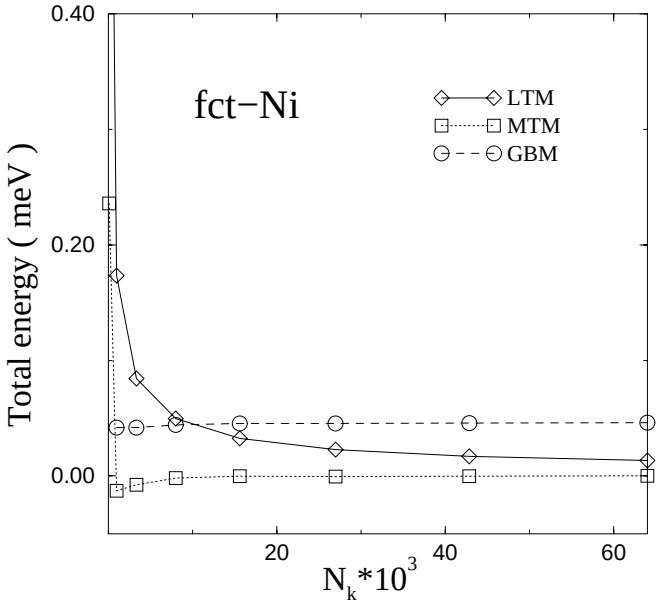

Fig. 1. Calculated total energy of fct Ni as a function of the number of **k**–points use for sampling the BZ. Three different sampling techniques were used, LTM, MTM and GBM (see text).

where $f_0(E,W) = \frac{1}{2}(1 - erf(\frac{E-E_F}{W}))$ (erf stands for error function) and A_n are coefficients which may be calculated analytically. In practical calculations one has to truncate the sum in the equation above and the resulting "step" function is called $f_N(E;W)$, if N terms are kept in the sum. If the function which is "smeared" by $f_N(E;W)$ (for instance the DOS times the energy – see equation (34)) can be represented by a polynomial of $2N$ there is no error involved in the truncation [30].

An example of how the different BZ integration methods work is show in Fig. 1 where the total energy of fct Ni (c/a ratio of 0.945) is presented as a function of the number of **k**–points in the irreducible wedge of the BZ [31]. The calculations were based on a full–potential linear muffin–tin orbital method, described in the next section. Note from Fig. 1 that the LTM converges much slower than the MTM and GBM. Notice also that the GBM does not converge to the same value as the other two methods which seem to converge to the same value. This is due to the fact that in the GBM the sum over Hermite polynomials is truncated, resulting in an approximate step function. However, the error in the energy differences is much smaller [31,32].

4.2 The FP–LMTO Method

We have outlined above a number of concepts which appear due to the translational symmetry of a solid, i.e. the Kohn–Sham equation must be solved for

a number of **k**–vectors which, for a given cycle in the self consistent loop, may be treated as independent of each other. In addition one has to find ways to approximate the **k**–space summation of the electron states and we have given examples of how one may do this. We are now ready to tackle the toughest part of the problem, namely to solve (27). One approach is to expand the (unknown) one–electron wave function in a set of (known) basis functions as,

$$\psi_{i,\mathbf{k}}(\mathbf{r}) = \sum_{l}^{l_{\max}} c_{li\mathbf{k}} \chi_{l\mathbf{k}}(\mathbf{r}). \tag{37}$$

The sum in the equation above is truncated after sufficiently many basis functions have been included and the coefficients $c_{li\mathbf{k}}$ are, via the Rayleigh–Ritz principle [16], determined from the following secular equation,

$$\sum_{l}^{l_{\max}} [H_{ll'} - E_{i\mathbf{k}} O_{ll'}] c_{li\mathbf{k}} = 0, \tag{38}$$

where

$$H_{ll'} = \int_{\mathrm{U_c}} \chi_{l\mathbf{k}}(\mathbf{r}) [\frac{-\nabla^2}{2} + V_{\mathrm{eff}}^{\uparrow(\downarrow)}] \chi_{l'\mathbf{k}}(\mathbf{r}) d^3r \equiv \int_{\mathrm{U_c}} \chi_{l\mathbf{k}}(\mathbf{r}) h_{\mathrm{eff}} \chi_{l'\mathbf{k}}(\mathbf{r}) d^3r \tag{39}$$

and

$$O_{ll'} = \int_{\mathrm{U_c}} \chi_{l\mathbf{k}}(\mathbf{r}) \chi_{l'\mathbf{k}}(\mathbf{r}) d^3r, \tag{40}$$

where the integral is over the unit cell ($\mathrm{U_c}$). Once $H_{ll'}$ and $O_{ll'}$ have been evaluated the eigenvalues, $E_{i\mathbf{k}}$ ($i = 1 - l_{\max}$), are determined by [16]

$$\det |H_{ll'} - E_{i\mathbf{k}} O_{ll'}| = 0, \tag{41}$$

a standard numerical problem, which may be solved by existing software.

4.3 Defining the LMTO Basis Functions

The difficulty is now to choose a basis set which is flexible and converges fast, i.e. as few basis functions as possible are needed to represent with sufficient accuracy a given eigenfunction, $\psi_{i,\mathbf{k}}(\mathbf{r})$. One efficient basis set is comprised of so called linear muffin–tin orbitals [10], which may be used in a full–potential mode, as described by Wills [33] or with the use of the atomic sphere approximation [10]. Both these methods are reviewed in other chapters of this book[34,35], hence we give only some of the details here.

Let us note here that the FP–LMTO method is defined using a base geometry, which is the usual construction of muffin–tin spheres centered around the atoms and a region outside these spheres, called the interstitial region. In

the muffin–tins, the basis functions, electron density, and potential are expanded in spherical waves, whereas in the interstitial, the basis functions, electron density, and potential are expanded in Fourier series. The calculation of the Hamiltonian and overlap matrix elements thus involves replacing the integrals in (39) and (40) with two parts, one coming from the muffin–tins and one coming from the interstitial. To be specific we break up integrals of $f(\mathbf{r})$ as $\int_{\mathrm{U_c}} f(\mathbf{r})d^3r = \int_{\mathrm{MT}} f(\mathbf{r})d^3r + \int_{\mathrm{Int}} f(\mathbf{r})d^3r$.

The basis functions used in the LMTO method are best described as augmented (or rather, inside the muffin–tin spheres, replaced) Bessel functions. These functions are described mathematically as,

$$\mathcal{K}_\ell(\kappa, r) \equiv -\kappa^{\ell+1} \begin{cases} n_\ell(\kappa r) - i j_\ell(\kappa r)\kappa^2 < 0 \\ n_\ell(\kappa r)\kappa^2 > 0 \end{cases} \tag{42}$$

$$\mathcal{K}_L(\kappa, \mathbf{r}) \equiv \mathcal{K}_\ell(\kappa, \mathbf{r})\mathcal{Y}_{\mathbf{L}}(\hat{\mathbf{r}}) \tag{43}$$

$$\mathcal{J}_L(\kappa, \mathbf{r}) \equiv \mathcal{J}_\ell(\kappa, \mathbf{r})\mathcal{Y}_{\mathbf{L}}(\hat{\mathbf{r}}) \tag{44}$$

$$\mathcal{J}_\ell(\kappa, r) \equiv j_\ell(\kappa r)/\kappa^\ell \tag{45}$$

In the equation above we have used,

$$\mathcal{Y}_{\ell m}(\hat{\mathbf{r}}) \equiv i^\ell Y_{\ell m}(\hat{\mathbf{r}}) \tag{46}$$

$$C_{\ell m}(\hat{\mathbf{r}}) \equiv \sqrt{4\pi\frac{2}{\ell}+1}\; Y_{\ell m}(\hat{\mathbf{r}}) \tag{47}$$

$$\mathcal{C}_{\ell m}(\hat{\mathbf{r}}) \equiv i^\ell C_{\ell m}(\hat{\mathbf{r}}), \tag{48}$$

where Y is a spherical harmonic.

4.4 The Muffin–Tin Matrix Element

The evaluation of matrix elements over the muffin–tin region requires a mathematical description of the basis function used in this part of the crystal. In case the effective potential in (24) is a constant (a purely hypothetical situation) the eigenfunctions can be written as plane waves or as a linear combination (a so called Bloch sum) of spherical Hankel or Neumann functions. To be specific the expression is (for a mono–atomic solid)

$$\chi_L(\mathbf{k}, \mathbf{r}) = \sum_{\mathbf{R}} \mathbf{e}^{\mathbf{ik}\cdot\mathbf{R}} \mathcal{K}_\ell(\kappa, |\mathbf{r} - \mathbf{R}|)\mathcal{Y}_{\ell\mathbf{m}}(\mathbf{r} - \mathbf{R}), \tag{49}$$

where $\mathcal{K}$ is a basis function defined in (42). Since part of the crystal has an effective potential which is rather constant, and does not vary much (in the interstitial) it is meaningful to use the above quoted functions as basis functions in the interstitial region. However, before describing how these functions are used to calculate (39) and (40) let us first deal with the muffin–tin region. We first note that (49)

$$\chi_L(\mathbf{k},\mathbf{r}) = \sum_{\mathbf{R}} \mathbf{e}^{\mathbf{ik}\cdot\mathbf{R}} \sum_{\mathbf{L}'} \mathcal{Y}_{\mathbf{L}'}(\hat{\mathbf{r}}) \; [\mathcal{K}_{\ell'}(\kappa, s_\tau)\delta(R,0)\delta(L,L') + \mathcal{J}_{L'}(\kappa, s) B_{L',L}(\kappa, \mathbf{R}),] \tag{50}$$

can be rewritten inside a muffin–tin sphere at $\mathbf{R}$=0 as a multi–pole expansion which yields,

$$\chi_L(\mathbf{k},\mathbf{r}) = \sum_{\mathbf{L}'} \mathcal{Y}_{\mathbf{L}'}(\hat{\mathbf{r}})(\mathcal{K}_{\ell'}(\kappa,\mathbf{s})\delta(\mathbf{L}',\mathbf{L}) + \mathcal{J}_{\mathbf{L}'}(\kappa,\mathbf{s})\mathbf{B}_{\mathbf{L}',\mathbf{L}}(\kappa,\mathbf{k})). \tag{51}$$

This function is continuous and differentiable at the muffin–tin spheres. Since the effective potential around the nuclei, inside the muffin–tins, is more or less spherically symmetric and atomic like an efficient choice of basis set is to replace the Bessel and Neumann functions in (50) with numerical functions that are solutions to a Kohn–Sham like differential equation. However, the numerical functions are only determined inside the region where the effective potential is close to being spherical, i.e. inside the muffin–tins. They are calculated from $\Psi = a\psi + b\dot{\psi}$, where $(h_{\text{eff}}^{\text{spherical}} - \epsilon_\nu)\psi = 0$ and $\dot{\psi}$ is the energy derivative of ψ. The constants a and b are determined to ensure continuity and differentiability. Hence the Bessel and Neumann functions are replaced, in a continuous and differential way, with numerical functions. The basis function to be used in the muffin–tin region is then,

$$\chi_L(\mathbf{k},\mathbf{r}) = \sum_{\mathbf{L}'} \mathcal{Y}_{\mathbf{L}'}(\hat{\mathbf{r}})(\Phi_{\ell'}(\kappa,\mathbf{s}_\tau)\delta(\mathbf{L}',\mathbf{L}) + \Phi_{\mathbf{L}'}(\kappa,\mathbf{s})\mathbf{B}_{\mathbf{L}',\mathbf{L}}(\kappa,\mathbf{k})). \tag{52}$$

With this basis function, matrix elements of the Hamiltonian and overlap can be evaluated over the muffin–tin region. Added to each such matrix elements is then the contribution from the interstitial region, which is described next.

4.5 The Interstitial Matrix Element

The basis function in the interstitial region is described by (49). However, since it has been found to be efficient to represent the effective potential and charge density as Fourier series, it becomes computationally efficient to make use of a Fourier series also for the basis function. This is possible since a basis function to be used in a crystalline environments can be written as a periodic function multiplied with a plane wave, and one can of course express the periodic function in a Fourier series. Hence one makes use of,

$$\chi_L(\mathbf{k},\mathbf{r}) = \sum_G \chi_G \mathrm{e}^{\mathrm{i}(\mathbf{k}+\mathbf{G})\cdot\mathbf{r}}, \tag{53}$$

in the interstitial region from which the interstitial contribution to the Hamiltonian and overlap matrix elements are evaluated. Since the potential in the interstitial region is represented as a Fourier series the evaluation of the matrix element of the Hamiltonian (and the overlap) becomes relatively simple, involving a sum of Fourier components. In practice it becomes faster to perform this integral via a combination of inverse Fourier transforms and Fourier transforms, which is not described here.

5 Magneto–Crystalline Anisotropy of Selected Materials

5.1 General Remarks

In the remaining part of this chapter we will give examples of how the theories outlined above can be used to calculate the magneto–crystalline anisotropy, as well as spin and orbital moments. However, before entering the details of this section which describes the magneto–crystalline anisotropy (MAE) as well as spin and orbital moments of selected materials, it should be mentioned that van Vleck pointed out, already in 1937 [36], that the spin–orbit interaction is responsible for the coupling of the spin to the lattice, which then gives rise to a magnetic anisotropy in a magnetic solid. Hence, much of the physical understanding of the mechanisms behind the MAE of 3d elements have been known for a long time. Actual calculations of the MAE have been thwarted because efficient methods for solving the Kohn–Sham equations, in combination with fast computers, are only recently available. Pioneering and important work in the field of MAE was also made by Brooks [37] and Kondorsii and Straub [38] where technical details of, for instance, problems with BZI were analyzed. We are interested here in the electronic contribution to the MAE, provided by the coupling of spin and orbital angular momenta, via the spin–orbit coupling. There is also another contribution to the MAE which is called the shape anisotropy (described in the following section). However, in the theoretical description of the MAE below we shall focus on the contribution given by the spin–orbit coupling. Hence, when comparing theory and experiment we have, unless otherwise explicitly stated, removed the shape anisotropy from the experimental data.

5.2 Shape Anisotropy

The shape anisotropy results from the magnetic dipole interaction. To calculate it we can consider a lattice of magnetic dipoles with magnetic moment μ_i. The energy of the dipole interaction can be written as [2] $E_{\rm dipole} = -\frac{1}{2}\sum_i \mu_i \cdot \mathbf{h}_i$, where $\mathbf{h}_i$ is the field intensity at lattice point i due to all the other dipoles. This interaction can be written as [39,40],

$$E_{\rm dipole} = \frac{1}{c^2}\sum_{i\neq i'}\Big[\frac{\mu_i\cdot\mu_{i'}}{|\mathbf{R}_i-\mathbf{R}_{i'}|^3} - 3\frac{(\mu_i\cdot\{\mathbf{R}_i-\mathbf{R}_{i'}\})(\mu_{i'}\cdot\{\mathbf{R}_i-\mathbf{R}_{i'}\})}{|\mathbf{R}_i-\mathbf{R}_{i'}|^5}\Big], \tag{54}$$

where $\mathbf{R}_i$ is a vector describing the lattice point i. Due to the long range nature of the magnetic dipole interaction the sum in (55) depends on the shape of the sample, and this leads to the shape anisotropy. For thin films, for instance, it always favors in–plane moments.

5.3 Orbital Moments and Orbital Polarization

An important part of magnetism, especially when considering the MAE, is the orbital contribution to the magnetic moment. Just as the spin moment can be written as the expectation value of s_z using the wavefunctions in (37) one can calculate the orbital moment from [41],

$$L_\sigma = \sum_{\mathbf{k}i} \left\langle \psi^\sigma_{i,\mathbf{k}}(\mathbf{r}) \left| l_z \right| \psi^\sigma_{i,\mathbf{k}}(\mathbf{r}) \right\rangle . \tag{55}$$

The expectation value in (55) is non–zero only if the relativistic spin–orbit coupling is included in the calculation and if the spin degeneracy is lifted. Via the spin–orbit interaction there is now a coupling between spin and orbital angular momentum and it is this interaction which is responsible for the electronic contribution to the MAE. Hence the orbital moment and the electronic contribution to the MAE have in common the fact that they both are a consequence of the spin–orbit interaction and below we will show that one can sometimes write an explicit relationship between the MAE and the orbital moment. From the arguments above it is clear that any theoretical method which attempts to calculate the MAE or orbital moment must consider the spin–orbit interaction. This can either be done by solving the Dirac equation, by use of perturbation theory, or to diagonalise a fully relativistic Hamiltonian using basis functions from a non–relativistic Hamiltonian [10,42] (or more precisely scalar relativistic Hamiltonian, since so–called scalar relativistic corrections such as mass velocity and Darwin shifts [23] are normally included in most band structure methods anyway). Using perturbation theory is more approximate than the other two methods, which give almost identical results[7]. The latter finding in not too surprising since the same relativistic Hamiltonian is considered, only the form of the basis functions is different. Diagonalising a relativistic Hamiltonian with scalar–relativistic basis functions has the advantage of being relatively easy and scalar–relativistic codes may, without too much effort, in this way be modified to include also the spin–orbit interaction. This can either be done in a straight forward way [10,42], as will be described below, or by using the so–called second variation approach [45]. The basic principle in these two implementations is however the same, and we describe only the first version here. If the effective

[7] This was found for instance when comparing orbital moments of Fe, Co and Ni calculated using these two different methods, but also by inspection of the DOS of Pu [44], a very heavy element where the spin–orbit interaction is approximately 1 eV.

Hamiltonian in (39) is augmented to include also the relativistic spin–orbit interaction, $h_{\text{eff}}^{\text{relativistic}} = h_{\text{eff}}^{\text{scalar}} + \xi \mathbf{l} \cdot \mathbf{s}$, (where ξ represents the strength of the spin–orbit interaction) the secular equation in (38) is modified as follows,

$$\sum_{l}^{l_{\max}} \sum_{\sigma} [H_{l\sigma l'\sigma'} - E_{i\mathbf{k}} O_{ll'} \delta_{\sigma\sigma'}] c_{l\sigma i\mathbf{k}} = 0. \tag{56}$$

In this equation matrix elements of the form

$$\langle \chi_{l\sigma\mathbf{k}}(\mathbf{r})\sigma \left| \xi \mathbf{l} \cdot \mathbf{s} \right| \sigma' \chi_{l'\sigma'\mathbf{k}}(\mathbf{r}) \rangle$$

$$\begin{aligned} &= \langle \chi_{l\sigma\mathbf{k}}(\mathbf{r})\sigma \left| \xi \left(l_x s_x + l_y s_y + l_z s_z \right) \right| \sigma' \chi_{l'\sigma'\mathbf{k}}(\mathbf{r}) \rangle \\ &= \left\langle \chi_{l\sigma\mathbf{k}}(\mathbf{r})\sigma \left| \xi \left(\frac{l_+ s_- + l_- s_+}{2} + l_z s_z \right) \right| \sigma' \chi_{l'\sigma'\mathbf{k}}(\mathbf{r}) \right\rangle, \end{aligned} \tag{57}$$

must be evaluated. Since the basis functions involve spherical harmonic functions, spinors,σ, and a radial component, these matrix elements are rather straight forward to calculate. Diagonalisation of (56) now yields eigenvalues which are not pure spin states. Instead, the wave function of a given eigenvalue is written as a linear combination of states with different l and σ character.

A practical complication of (57) is that the Hamiltonian matrix is doubled in size, making the numerical diagonalisation procedure slower. A further complication of including both the spin–orbit coupling and a lifting of spin degeneracy is that the symmetry (of the crystal) is reduced. Consider for example a cubic crystal, such as bcc Fe. Normally there are 48 point group operations which leaves the lattice invariant. However, if magnetism is considered and if the magnetization is coupled to the lattice via the spin–orbit interaction, the so–called double group [46] has to be considered, and the effect of the time reversal operator has to be taken into consideration. If the magnetization of our cubic lattice is pointing along the crystallographic z–axis we can, for instance, not perform a 90 degree rotation around the x- or y–axis, since the magnetization direction then is rotated out from the z–axis and the system is not invariant. However, a 90 and 180 degree rotation around the z–axis is allowed. Also, a 180 degree rotation around the x–axis flips the magnetization direction from the z–direction to the z–direction and in itself such a symmetry operation is not allowed. However, the product of this rotation and the time reversal operator (which changes the sign of the magnetization) is an allowed operation and this element of the double group does leave the crystal invariant. Our example of a cubic lattice when the magnetization is pointing along the z–direction has 16 allowed symmetry operations. Hence, the lattice becomes tetragonal in symmetry, an effect which we will discuss below in connection with calculations of magneto–striction. At present we simply note that the reduced symmetry simply means that the irreducible part of the BZ is larger, and that more $\mathbf{k}$–points need to be sampled in order to have a well converged total energy.

Since the spin–polarization (spin pairing) is treated via a spin–dependent effective potential, such as (29), and the relativistic spin–orbit interaction is

treated via (57), the physical mechanisms behind Hund's first and third rules, respectively, are (at least approximately) included. One can at this stage ask the question why total energy calculations based on different approximations of DFT ignore Hund's second rule? The answer to this question is of course that an exact formalism for including effects responsible for Hund's second rule is lacking at present. However, it has been pointed out [47] that an approximate way to incorporate Hund's second rule in total energy calculations, using DFT, is to add to the LDA (or GGA) energy functional a term,

$$E_{\mathrm{OP}} = -\frac{1}{2}\sum_{\sigma} E_{\sigma}^{3} L_{\sigma}^{2}. \tag{58}$$

In this equation E_{σ}^{3} is the so called Racah parameter (note that this parameter is normally denoted B for d–electrons and E^3 for f–electrons), which may be calculated from Slater integrals; F^2, F^4 and F^6 [48,49]. The correction in (58) is normally referred to as the orbital polarization (OP) correction. This form for including electron–electron interactions comes from the finding that a vector model, involving interactions of the form $l_i \cdot l_j$ between electron pairs [50,51], can be used to calculate the lowest energy multiplet. In fact an explicit expression for electron–electron interactions having a term $l_i \cdot l_j$, is quoted both by van Vleck [50] and Ballhausen [51]. This term in the electron–electron interaction was also used by Norman et al. [52] to give a correction term which is similar to the form in (58). Summing the interaction, $l_i \cdot l_j$, over electron pairs as well as replacing the average of this interaction with the sum over average interactions, $l_{zi} l_{zj}$, gives rise to an expression for orbital correlations given by (58) [47]. The approximation of replacing $l_i \cdot l_j$ with the average is in the spirit of replacing the spin pairing energy, $\sum_{i \neq j} s_i \cdot s_j$, with a Stoner expression $\sum_i s_{zi} \sum_j s_{zj} = S_z^2$. Since this form of the energy is absent in the LDA or GGA energy functionals one must add the energy of (58) to these total energy functionals. The interactions which are responsible for Hund's second rule, which in physical language are a reflection of that states with different angular momentum have different angular shape and hence a different Coulomb interaction, are now in an approximate way included in the energy functional.

To illustrate the importance of (58) we show in Fig. 2 the energy correction corresponding to (58) for the 4f electrons of the lanthanide atoms (or ions). Specifically Fig. 2 shows equation (58) neglecting the effect of E^3, hence illustrating only the angular behavior of the correction. The correction in (58) is compared to the exact values [53], which are calculated from the energy difference between the lowest atomic multiplet of the f^n configurations and those corresponding to the Grand Barry Centre (an average of the multiplets). This energy difference involves of course also spin–pairing energy and spin—orbit interaction, but shown in Fig. 2 is only the part which depends on the orbital angular momentum. To get a feeling for how important the correction in (58) is, we note that for a rare–earth system the value of E^3 is ˜5 mRy which means that the correction in (58) can be as large as ˜100 mRy. From Fig. 2 we note that the agreement between the approximate form of the orbital part of the electron–electron inter-

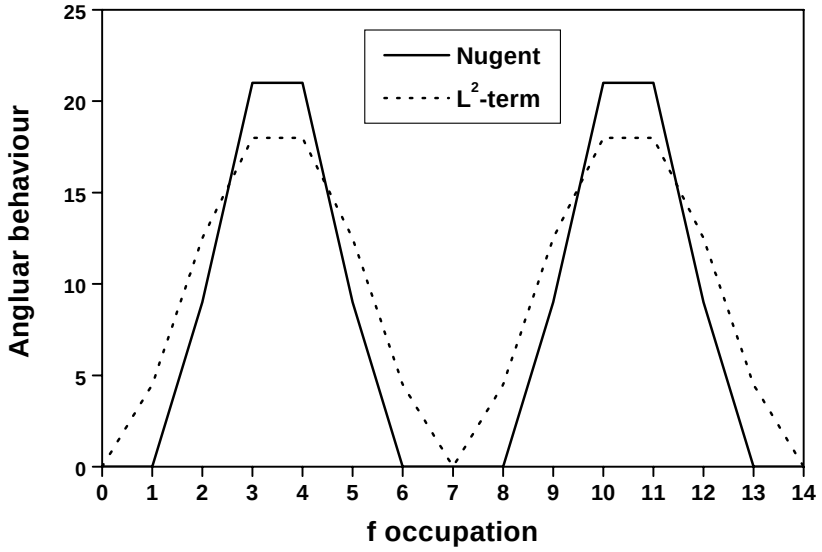

Fig. 2. Angular behavior of the electron–electron interactions of the f–elements, as given by Nugent [53] and from equation (58).

action, given in (58), and the exact values given by Nugent [53] is rather good. The largest disagreement is found for an f–occupation close to 1, 6, 8, and 13, since the exact values should be zero here (there is for instance no spin- and orbital pairing energy of a single electron), whereas the approximate correction does yield a non–zero correction. This is analogous to the fact that LSDA gives a spin–pairing energy of a single electron system.

The derivation of (58) was made having nearly localized electron systems in mind [47] and for other systems other corrections should be tried. We have previously mentioned the corrections of Norman [52], but there is also a third form suggested by Severin and co–workers [54]. We will not describe all the proposed corrections in detail here, but instead quote some results of calculations using (58), in order to illustrate the importance of these types of corrections, not only for f–electron systems but also for d–electron systems and in particular for orbital magnetism. In Figs. 3 and 4 we show the calculated spin and orbital moments [55], respectively, of Fe, Co and Ni, including alloys between these elements. The calculations were using a standard LSDA calculation (with spin–orbit interaction), as well as the correction in (58). In the figures experimental values are also shown, and we note that an improved agreement between theory and experiment is consistently found for the orbital moment, when the OP correction is used. This is encouraging as well as reasonable, since the correction is supposed to include an interaction which is present in an interacting electron system. In

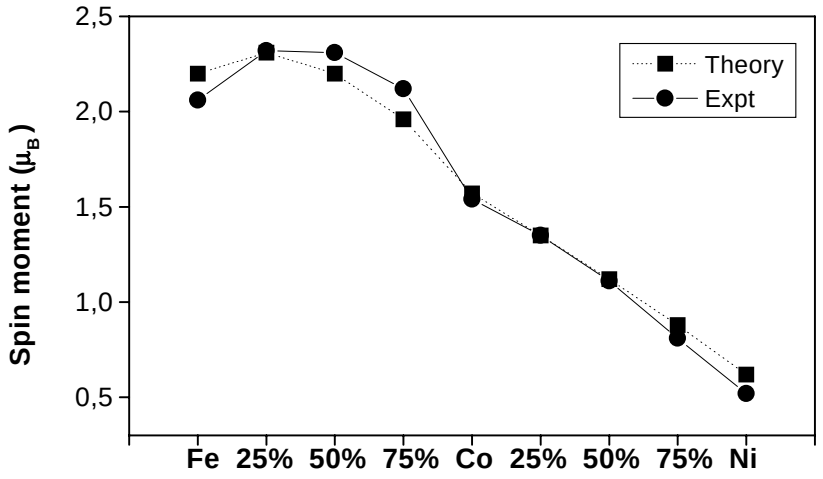

Fig. 3. Calculated and experimental values of the spin moments of the 3d elements, Fe, Co and Ni, as well as for alloys between them.

addition we also observe that the orbital moments show a rather irregular behavior and as discussed by Söderlind [55] this is due to band filling effects. Since the size of the orbital moment is to a large degree caused by a redistribution of electron states around the Fermi level, [56,57] it generally scales to some degree with the value of the DOS at $E_{\rm F}$. Hence a large DOS at $E_{\rm F}$ normally results in a larger orbital moment and the irregular behavior of the orbital moment is to some degree a reflection of an irregular behavior of the DOS at $E_{\rm F}$, for these alloys. In addition the crystal symmetry is important since hcp Co is found to have the largest orbital moment. It can be argued from perturbation theory that for a cubic material the influence of the spin–orbit coupling strength, ξ, enters as ξ^4. For non–cubic materials the dependence is stronger, and this generally results in larger orbital moments.

6 MAE of 3d Elements

6.1 Fe, Co and Ni

The first example of calculated MAE values which we would like to discuss is at first glance the simplest, namely the MAE of the ferromagnets Fe, Co and Ni. However, due to that the MAE is extremely small for these elements, at least for bcc Fe and fcc Ni (of order μeV) the task of calculating this from first principles

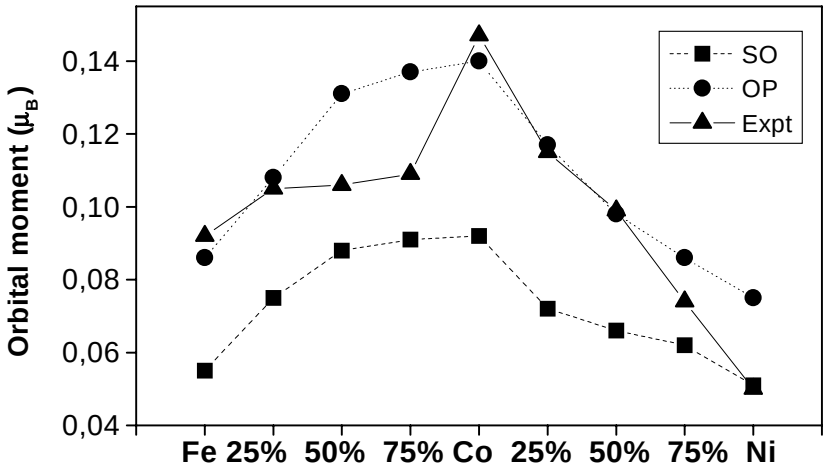

Fig. 4. Calculated and experimental values of the orbital moments of the 3d elements, Fe, Co and Ni, as well as for alloys between them. Calculations with (OP) and without (SO) the orbital polarization term are shown.

is enormously difficult, where especially a high accuracy of the computational method is needed as well as a very dense sampling of the BZI. For this reason different values of the MAE of bcc Fe, hcp Co and fcc Ni have been reported in the literature. Some of the most recently calculated [58] values of the MAE are listed in Table 1.

Table 1. MAE of Fe, Co and Ni in different crystal structures. All units in μeV. The MAE is calculated as the difference between the axis: 001-111 for the bcc Fe, 001-100 for the hcp Co, 001-111 for the fcc Co and finally 001-111 for the fcc Ni.

MAE	bcc Fe	hcp Co	fcc Co	fcc Ni
ASA-force theorem [40]	-0.5	16	-	-0.5
ASA-total energy [60]	-2.6		2.4	1.0
FP-total energy [58]	-0.5 (-1.8)	-29 (-110)	0.5 (2.2)	-0.5 (-0.5)
experiment	-1.4	-65	1.8 [59]	2.7

In the Table 1 we quote results obtained using the atomic sphere approximation (ASA) where spherical potentials in overlapping spheres are used to replace the actual effective potential of the lattice (in equation (29)) in combination with

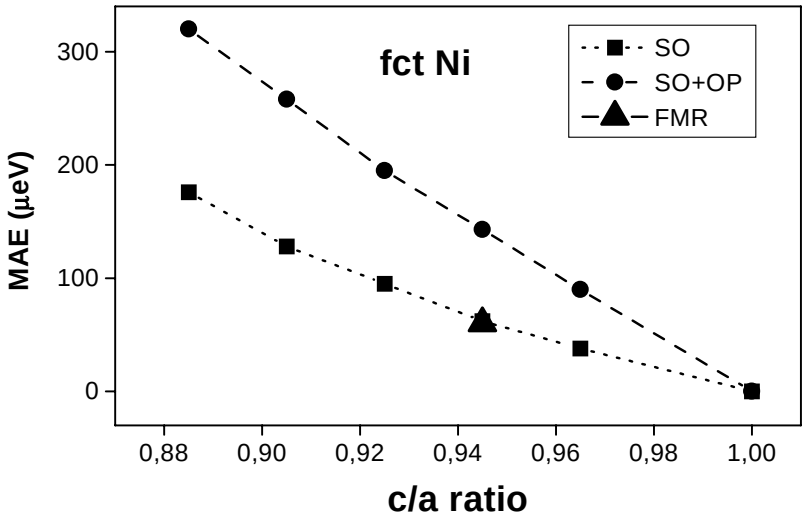

Fig. 5. Calculated and experimental values of the MAE of bcc Fe (001 vs. 111 direction), hcp Co (0001 vs. 100 direction), fcc Co (001 vs. 111 direction) and fcc Ni.(001 vs. 111 direction). Calculations with and without the orbital polarization term are shown.

a minimal basis set. This approximation is estimated to give an error in each calculated eigenvalue of a few mRy's [10]. The full potential (FP) calculations make no approximation to the shape of the charge– or spin density as well as the shape of the effective potential (equation (29)) and as described above makes use of a double or sometimes even a triple basis set. One may note from Table 1 that a variety of signs and sizes of the MAE may be obtained for Fe, Co and Ni, depending on which approximation one uses. The calculations of Ref. [40] seem to be well converged with respect to the number of **k**–points used, as do the calculations of Ref. [60]. Since both these methods use the ASA the disagreement in the MAE of bcc Fe and fcc Ni must be caused by the use of the so called force theorem[8] in Ref. [40]. This finding is consistent with the analysis of Ref. [62] where it was argued that for cubic systems the applicability of the force theorem may be limited. In the Table 1 we have quoted a value of 16 μeV for hcp Co, using ASA and the force theorem. This actually corresponds to the wrong easy axis. However, this value was obtained using an spdf basis set, whereas an spd

[8] The force theorem [61] states that the total energy difference between two different magnetization directions may simply be calculated from the difference in the eigenvalue sum of the the two magnetization directions, using the same effective potential for the two directions. This approximation is correct to first order changes in the charge and magnetization density.

basis set gave a value of -29 μeV, i.e. the correct easy magnetization direction. One can possibly draw the conclusion from this finding that the MAE of hcp Co is hard to converge with a minimal basis set. Unfortunately no total energy calculation using the ASA [60] was reported for hcp Co so that one can not examine if the poor convergence in the number of basis functions is connected to the use of the force theorem or not. The total energy, full–potential calculations did report on convergence tests with respect to the number of **k**–points, the width of the Gaussians used in the GBM for the BZI and the basis functions used (however, mostly for Ni). In fact the convergence of the double basis set (which is a standard size of the basis set of FP–LMTO calculations) was tested by a calculation which adopted a triple basis set (i.e. three s basis functions, three p basis functions and three d basis functions, each connecting to an envelope function with a unique kinetic energy). Since the full–potential calculations have the most flexible basis set as well as a more exact effective potential (29) these results must be considered as the most accurate of the ones in Table 1[9]. If we now examine the MAE values of Table 1, using the full–potential method, we find that the correct easy axis is found for all elements except fcc Ni. We also note that including the OP influences the size of the MAE quite strongly, as it did for the orbital moments in Fig. 4. In order to show this dependence more clearly we compare in Fig. 5 different calculated MAE values (using the FP–LMTO method) with experimental data. Note that for bcc Fe and fcc Co including the OP correction improves the agreement with experiment, whereas for hcp Co the experimental value is between the two different theoretical values.[10] For fcc Ni the OP correction has a very small effect on the MAE and the 001 axis is calculated to be the easy axis, in disagreement with observations. As we shall see below, where more examples are given, first principles calculations normally reproduce the correct easy axis, even if the size of the MAE may deviate somewhat. The fact that first principles calculations, based on the LSDA, are incapable of providing the correct easy axis for fcc Ni is probably connected to deficiencies in the form of the exchange and correlation potential in LSDA. From Table 1 and Fig. 5 we also note that the effect of crystal symmetry has a large influence on the size and direction of the MAE, since Co in the fcc phase has a much smaller value of the MAE compared to the value of the hcp phase. This can be understood from perturbation theory where, as stated, it is known that due to the high symmetry of the cubic crystal structure the influence of the spin–orbit coupling strength (ξ) on the MAE enters as ξ^4. Since the value of ξ is rather small for Fe, Co and Ni, it follows that in cubic phases the magnitude of the MAE is tiny. For lower symmetries of the crystal a stronger interaction of ξ on the MAE is present, resulting in larger MAE values.

[9] Although this statement was debated in Ref. [60] we maintain that these arguments are not valid and the tests made to compare the two methods [60] are of poor quality.

[10] Recent work by P. James [63] show that a better converged calculation of hcp Co yields a MAE value of $\sim$ 20 μeV when the OP correction is omitted, with the 001 axis as the easy direction.

6.2 Effects of Straining the Crystal Structure

In this section we discuss theoretical results of the MAE and spin and orbital moments of tetragonally strained Fe (bct), Co (fct) and Ni (fct). Many studies of orbital magnetism and MAE are devoted to Fe, Co and Ni as over–layers on a substrate with a small in-plane lattice mismatch. This causes a strain in the over-layer material (Fe, Co or Ni) for thicknesses sometimes up to 50 atomic layers. As a rule of thumb one can estimate this strain by equating the in–plane lattice parameter to that of the substrate, then the out–of–plane lattice parameter of the over–layer is adjusted so that the volume/unit cell of the over–layer is constant and the same as for the elemental form of the over–layer material. The effect of strain on the MAE can, as we shall see in a moment, be large and since many experimental studies are devoted to studying this situation it is important to have a theoretical understanding of how crystallographic strain and MAE are connected.

In this section we have chosen one primary example for which there are both theoretical and experimental data available; Ni on Cu (001) [64]. A few recent LEED studies of Co and Ni films on Cu(001) [65,66]have shown that these films can be grown epitaxially in a face centered tetragonal (fct) structure which deviates with a few percent from that of the fcc structure. In addition these films have been shown to have an out–of–plane magnetization for film thicknesses *above* ˜7 atomic mono–layers [67] and an in–plane magnetization for thinner thicknesses [68]. This is a rather unusual behavior since in most systems the shape anisotropy will be the dominating term in the thicker limit and it always favors the in-plane magnetization. In many epitaxially grown magnetic films it is known that the magnetic anisotropy energy, MAE, (per atom) of the system can be expressed by the empirical formula, $E = E_{\rm v} + \frac{2E_{\rm s}}{n_d}$, where n_d is the number of atomic layers in the film and $E_{\rm v}$ and $E_{\rm s}$ are the so–called volume and surface (interface) contributions to the magnetic anisotropy energy, respectively. Normally the surface contribution ($E_{\rm s}$) is much larger than the volume contribution ($E_{\rm v}$) so that for thin film thicknesses the surface dominates and determines the easy axis magnetization. Normally the volume contribution is assumed to be a result of the material in an undistorted structure (e.g. fcc) and hence is assumed to be small. For instance the volume contribution of fcc Ni is small compared to the surface contribution. Hence only two terms need be considered, the surface contribution to the MAE and the shape anisotropy. With increasing film thickness the surface contribution becomes less important since it scales with the inverse of the film thickness, so that eventually the shape contribution dominates. Since this contribution always favors an in–plane magnetization, a change of magnetization direction as a function of increasing film thickness will be from out–of–plane to in–plane, in contrast to the experimental result for Ni on Cu. It was speculated [67] that the unusual behavior of the Ni/Cu system is driven by a large and positive volume contribution, $E_{\rm v}$, to the magnetic anisotropy energy in the Ni film which occurs due to the tetragonal distortion of Ni grown on a Cu(001) substrate, in combination with a negative surface contribution, $E_{\rm s}$. We

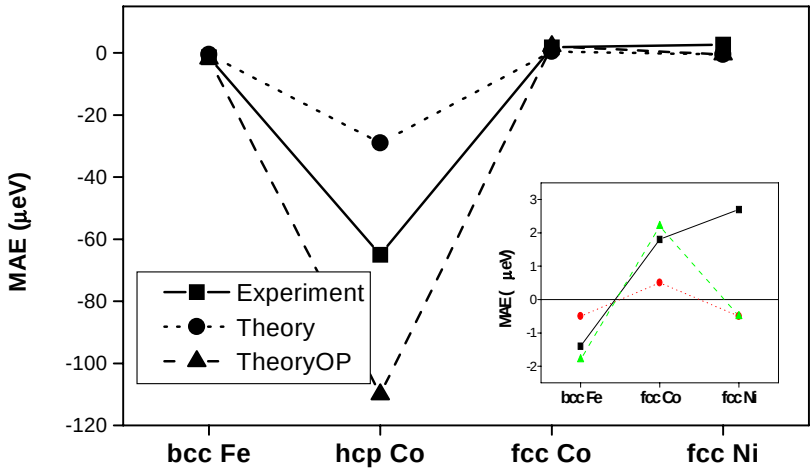

Fig. 6. Calculated values of the MAE (001 vs. 110 direction) as a function of crystallographic strain of fct Ni. Calculations with and without the orbital polarization term are shown. Also shown is the experimental value of Ref. [67].

will demonstrate in this section that this indeed is the case and that a breaking of the crystal symmetry enhances the value of the MAE dramatically.

Using the full–potential LMTO method, E_v for Ni in a face centered tetragonal (fct) structure was calculated [64]. E_v is here defined as the difference in total energy, between the [110] and [001] magnetization directions, per atom. In Fig. 6 E_v is plotted as a function of tetragonal strain, or equivalently c/a-ratio, of the fcc lattice (in reality it is, due to the strain, an fct lattice), assuming a constant in–plane parameter (i.e. this distortion is not volume conserving). (The in–plane lattice parameter, is designated 3.58 **r**A, which is the same as the value measured by LEED for thin Ni films on Cu [65]. The experimental lattice parameter of bulk fcc Ni is 3.52 **r**A). At c/a=1.0 the fct crystal has a volume which is larger than the volume of bulk fcc Ni. For comparison, both the calculated E_v with and without orbital polarization is shown. Note the large increase of E_v due to the orbital polarization. It is found that the [001] direction is the easy direction for all c/a <1.0. Further, we notice that E_v is linear in c/a, to first order, especially when c/a is close to 1.0. This indicates that our distortions in the range c/a ˜0.88 to 1.0 are in the magneto–elastic regime. Notice also that in the calculations with only the spin–orbit interaction included, this linear behavior is not as pronounced. In addition it may be observed that due to the breaking of the cubic symmetry the value of the MAE becomes very large. In

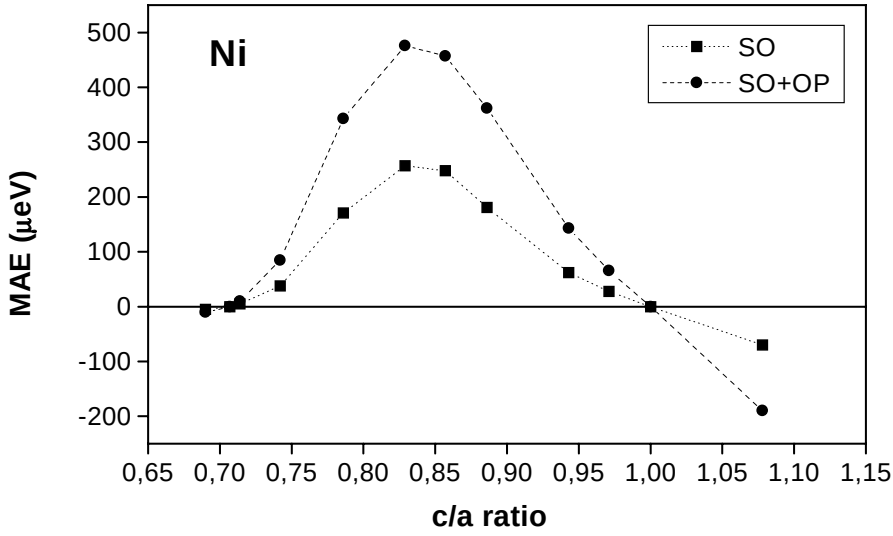

Fig. 7. Calculated values of the MAE (001 vs. 110 direction) of Ni, for strains along the Bains path. Calculations with and without the orbital polarization term are shown.

the figure we have also displayed one experimental value obtained from FMR experiments [64]. In Fig. 6 we see that, for the experimental value of the c/a ratio (c/a=0.945, corresponding to the tetragonal distortion in Ni films on Cu(001)), the theoretical calculation gives $E_{\rm v} = 140$ μeV. This is in reasonable agreement with the measured value, $E_{\rm v}$=60 μeV. The most important thing to note is that theory and experiment agree on the sign of $E_{\rm v}$ and that they both show that it is substantial in tetragonal Ni. As previously discussed by Schulz and Baberschke [67], the large and positive $E_{\rm v}$ term is larger than the shape anisotropy for the same Ni film. This leads to a change in magnetization direction for film thicknesses larger than a critical thickness of ˜7 mono–layers (i.e. $E_{\rm v}$ dominates over the negative surface term, $E_{\rm s}$, and the shape anisotropy), which is consistent with observations.

Since Fig. 6 demonstrates that a strain of the fcc crystal structure influences the value of the MAE very strongly it is of interest to investigate the MAE over large regions of strain. The so–called Bains path, which connects the bcc and fcc structures via a tetragonal strain, is especially useful here since one may calculate the MAE along the Bains path and observe how it is modified with respect to changes in the strain. For this reason we show in Fig. 7 calculated values of $E_{\rm v}$ along the Bains path. The calculations were done in such a way that the volume is the same for all different c/a ratios. For c/a close to fcc or bcc one observes an almost linear behavior as expected from magneto-elastic arguments. Since both

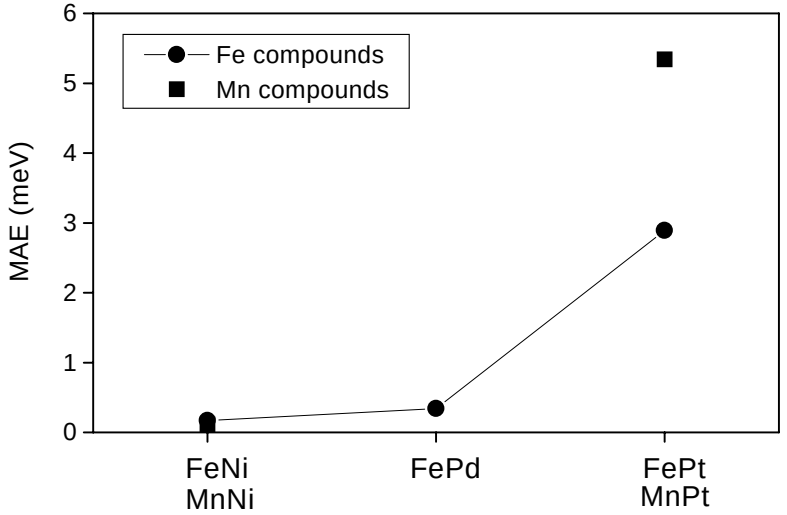

Fig. 8. Calculated values of the MAE (001 vs. 110 direction) of fct Ni as a function of calculated values of the orbital moment anisotropy. The behavior of (59) is shown as a straight line.

fcc and bcc are cubic structures, and therefore (for symmetry reasons) can only have magnetic anisotropy constants of 4^{th} order and higher, E_{v} must be small for c/a close to 1.0 and $\frac{1}{\sqrt{2}}$. Therefore the E_{v} curve must deviate from the linear behavior at some intermediate c/a ratio. In Fig. 7 it is seen that this happens when c/a is between 0.8 and 0.9. Further we notice that E_{v} is positive in the interval $\frac{1}{\sqrt{2}}<\mathrm{c/a}<1$ and negative for $\mathrm{c/a}>1.0$ and $<\frac{1}{\sqrt{2}}$. It seems likely that this information can serve as a prediction of the volume contribution to the MAE, of pseudomorphically grown tetragonal Ni films on any substrate (if possible to fabricate). Due to the elasticity the volume of fct Ni will never deviate much from the volume of fcc Ni and the curve in Fig. 7 should resemble the experimental reality.

6.3 The Correlation between MAE and Orbital Moment

An alternative to measuring the MAE directly (which could be difficult in certain cases) may be found from a simple relationship between the orbital moment anisotropy (OMA), which is defined as the difference in the orbital moment when the magnetization is pointing in two different directions and the total energy difference between these two directions, i.e. the MAE. Bruno showed [3], using perturbation theory and assuming that the exchange–splitting is larger

than the band width, that the following relationship holds between MAE and OMA,

$$MAE = \frac{\xi}{4\mu_B} OMA, \tag{59}$$

where ξ is the spin–orbit parameter. Hence instead of measuring the MAE of a system one could measure the orbital moment when the magnetization is pointing in one direction and subtract the measured orbital moment of a different magnetization direction. Forcing the magnetization to lie in a specific direction may be obtained by an applied external field. Hence, if it is judged that the OMA is easier to measure than the MAE one could simply take the measured OMA and use (59) to estimate the MAE. In addition this relationship may be used to analyze the behavior of measured MAE values of compounds, interfaces and so on. Since the relationship between OMA and MAE relies on different assumptions it is of interest to investigate how well this relationship holds for different systems. We present one example here, Ni on Cu, and show that the relationship between MAE and OMA actually is linear, which is what (59) suggests. To illustrate this we plot in Fig. 8 the MAE of fct Ni (the same calculation as described in the section above) as a function of the difference in orbital moment (OMA) when the magnetization is pointing in the 001 and 110 direction. Since the calculation of fct Ni was made for several values of the c/a ratio, several different values of both the MAE and OMA may be calculated and it is these data which are shown in the figure. The relationship between MAE and OMA are also shown in Fig. 8, using a value of 105 meV for ξ. Overall, the relationship between the MAE and OMA is roughly linear although for certain c/a ratios there are larger disagreements. This probably implies that the assumption of an exchange splitting which is larger that the band width is starting to break down.

7 Selected Compounds

There can be quite strong modifications of the MAE as well as spin and orbital moments when a 3d element is situated in a compound. A good understanding of the mechanisms which modify the MAE in one direction or the other is important since one then can start tuning material parameters in order to optimize the magnetic properties. We will outline here some observed trends and explain their origins. We illustrate this with some recent results by Ravindran et al. [69] on the FeX and MnX compounds (X=Ni, Pd and Pt).

7.1 FeX and MnX Compounds (X=Ni, Pd or Pt)

The MnX and FeX compounds crystallize in a layered tetragonal structure with two atoms per primitive unit cell. Experimentally the MAE has been measured for a large number of compounds of this type, some which are compiled in Ref.

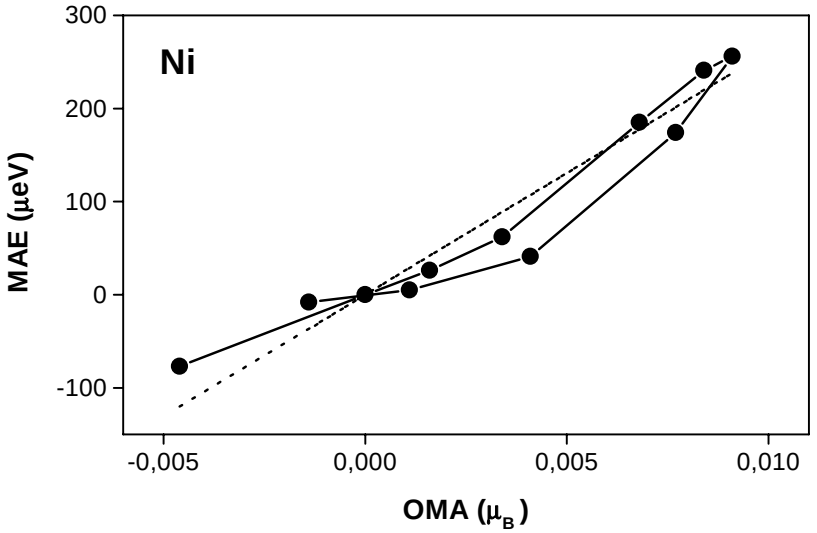

Fig. 9. Calculated values of the MAE (001 vs 100) of FeX and MnX compounds (X=Ni, Pd or Pt).

[69]. We will by no means report on all the details of the theoretical work of Ref. [69] but merely quote the results which are of largest importance for the discussion here. In Fig. 9 we show the calculated MAE of iso–structural FeNi, FePd and FePt as well as of MnNi and MnPt. This figure illustrates that for inter–metallic compounds the influence of the spin–orbit coupling of the ligand atom strongly influences the MAE. This finding was also observed for multi layer systems [70]. In particular one observes that a larger spin–orbit coupling of the ligand atom results in a larger value of the MAE. The reason for this is that the magnetism of the 3d atoms will induce a magnetic moment also in the ligand atoms, even if these atoms are non–magnetic as pure elements.

In Fig. 10 the effect of the exchange–splitting of the 3d atom is illustrated and we observe that a larger exchange–splitting results in a larger MAE. Since the MAE is a result of spin–orbit coupling in combination with spin polarization the results in Figs. 9 and 10 are maybe not too surprising but it is not entirely obvious that there should be a rather smooth relationship between the MAE and exchange–splitting, as Fig. 10 shows. All details of the calculated results for all studied FeX and MnX compounds are reported in Ref. [69] and are not given here. However, we note that theory obtains the correct easy axis of magnetization for all these compounds [69], although the absolute values sometimes deviate from experiments with as much as 50%.

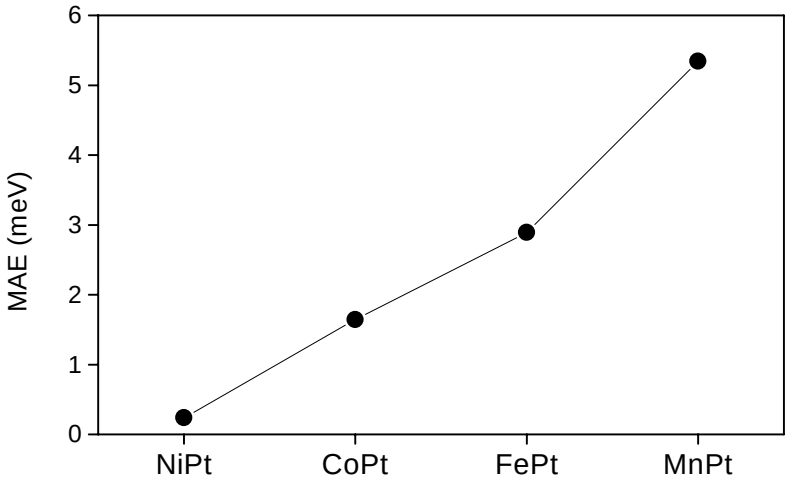

Fig. 10. Calculated values of the MAE (001 vs 100) of TPt (T=Ni, Pd or Pt).

8 Surface and Interface Magnetism

When an atom is close to an interface or a surface it will experience a different environment compared to its elemental environment and as a consequence, the wave function overlap between atoms, the hybridization and the direct hopping will be different. In short, the electronic structure will be modified. In this section we will illustrate how this rearrangement of the electronic structure produces magnetic properties such as spin and orbital moments and in addition how it modifies the MAE. These effects are possible to measure on an almost atomic level. For instance, the surface contribution to the MAE and the spin and orbital moments have been measured [66,67,71,72]. In addition to describing some arcetypal features of surface and interface magnetism we will illustrate with a few examples how, from an electronic structure point of view, one can use the knowledge of these modifications in order to influence the magnetic properties in a desired direction.

8.1 Spin and Orbital Moments of Selected Surfaces and Interfaces

The example to be discussed in this section is that of Co grown on Cu (001) [71]. This system is chosen since it is known experimentally that thin films of Co grow in a well characterized way (fcc) for up to 50 atomic layers, which enables measurement of the thickness dependence of the spin and orbital moments. In

the experiments of Tisher et al. [71]. X–ray dichroism was combined with the sum rules [73], which connect x–ray dichroism to the size of magnetic moments. The advantage with this experimental technique is that it gives atom specific information about the magnetism. By studying the thickness dependence of the ratio between orbital and spin moment one can calculate the interface, bulk and surface contribution to this ratio. The so obtained ratio between orbital and spin moments are in Table 2 compared to theoretical values [71]. Note that both for the interface and the surface the ratio between orbital and spin moments is increased over the bulk value. Theory is in good agreement with this finding, and the observed trend with the largest ratio between orbital and spin moments for the interface and smallest ratio for bulk, is reproduced by theory. Table 2 also lists the individual spin and orbital moments for the bulk, interface and surface atomic layers. As may be observed both the spin and orbital moments are enhanced for atoms which have a chemical surrounding which differs from bulk. However, the enhancement is larger for the orbital moment than it is for the spin moment. The enhancement of the spin moment may simply be understood from the fact that atoms which are close to the surface or close to the Co/Cu interface have a reduced number of nearest neighboring atoms. From a simple tight binding model, where the band width scales as the square root of the coordination number, the reduced bandwidth and enhanced spin moments at a surface or even an interface (if the interaction–hybridization between the atoms is weak over the interface) may be understood.

Table 2. Spin and orbital moments for 1 ML of Co on Cu (001), bulk fcc Co and Co surface (001).

quantity	1 ML Co/Cu (001)	Co (fcc, bulk)	Co (fcc, surface)
$M_L(\mu_B)$	0.261	0.134	0.234
$M_S(\mu_B)$	1.850	1.724	1.921
M_L/M_S (theo.)	0.141	0.078	0.122
M_L/M_S (expt.)	0.195	0.078	0.113

In Fig. 11 we display as an example the DOS of bulk fcc Co and the DOS projected on a Co atom for a mono–layer of Co on Cu (001). The narrowing of the DOS at the surface is clear from this figure. Hence, since reduced bandwidths almost always (but curiously not always) produce enhanced spin moments, the trends of the spin moments in Table 2 may be understood. Before entering the discussion about orbital moments we remark here first on the fact that even though the DOS at, for instance, a surface may become substantially more narrow compared to bulk, details of the filling of the bands as well as the hybridization with the underlying substrate may in rare cases produce reduced moments. An example of this is Ni on Cu (001) [74]. Let us now turn to the enhancement of the orbital moment at the interface and at the surface. For the surface it has been pointed out that the crystal field is different and that hence

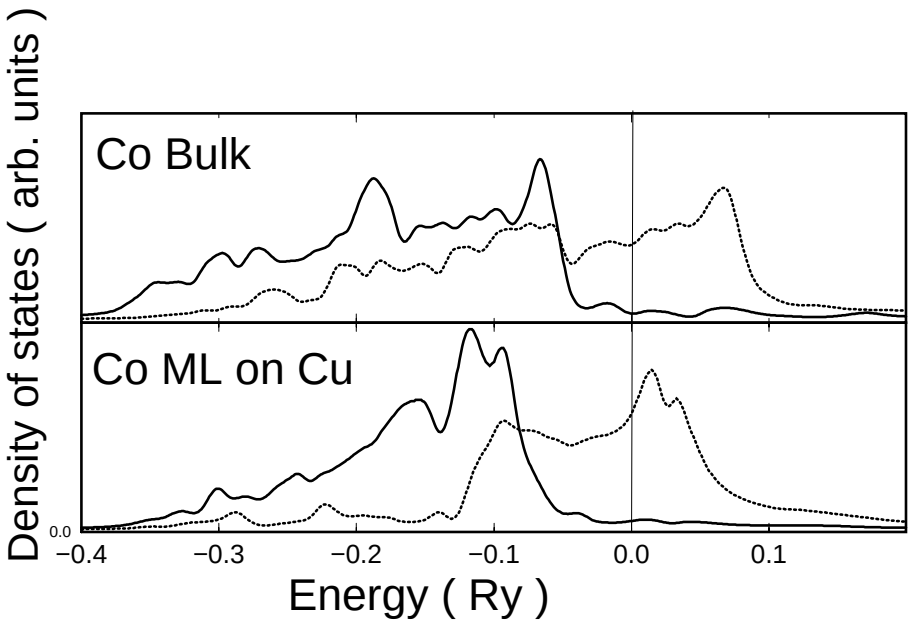

Fig. 11. Calculated density of states of bulk (hcp) Co and a Co monolayer on Cu (001). The Fermi level is marked by a vertical line.

the crystal field quenching is reduced at the surface [75]. This tends to enhance the orbital moments. Moreover, since the bands become more narrow at the surface the value of the DOS at E_{F} is enhanced compared to bulk producing larger orbital moments. Finally we observe that orbital moments appear only when one theoretically includes the relativistic spin–orbit interaction in a spin polarized calculation. A spin degenerate calculation, even if it includes the spin–orbit interaction, will yield a zero orbital moment. Thus, a spin moment which is reduced, approaching zero, produces an orbital moment which also is reduced and approaches zero. Conversely, increased spin moments, such as the ones for the surface and interface in Table 2, generally produce larger orbital moments. We have thus identified three mechanisms which for atoms at, or close to, the surface result in enlarged orbital moments. For the interface atoms all the above applies, and using these arguments one may also expect enhancements, at least if the interaction (hybridization) with the atoms across the interface is sufficiently small. Previously we discussed the simple relationship between MAE and OMA. Since the size of the orbital moments often is larger for surfaces and interfaces it is likely that the orbital moment anisotropy (OMA) also is enhanced, from which it follows that the value of the MAE is larger than it would be in the bulk. In addition to this the symmetry is lowered and the spin–orbit interaction influences the MAE more strongly (than ξ^4) which also produces larger values of the MAE at surfaces and interfaces.

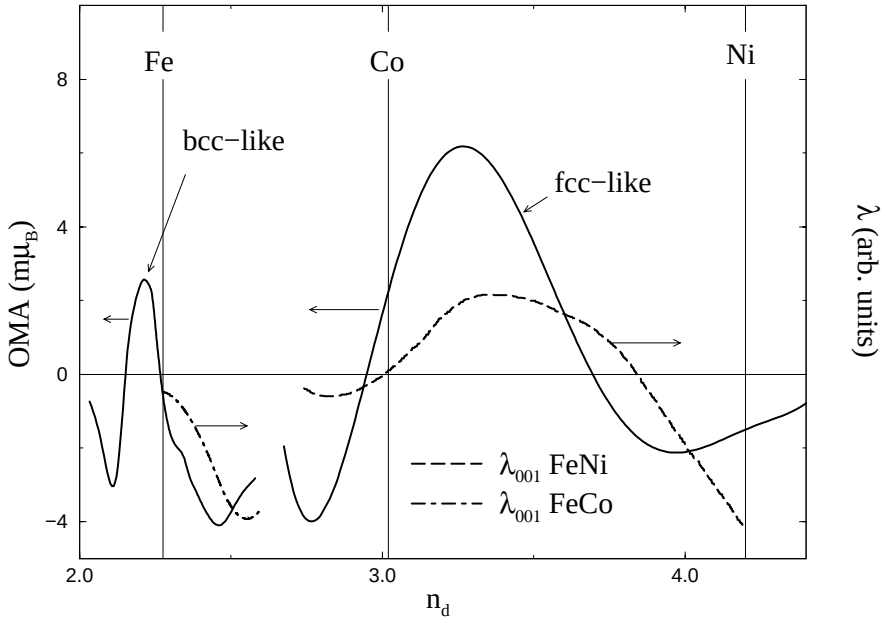

Fig. 12. Calculated OMA (full line, see text) and experimental magneto–striction coefficient of FeCo (bcc, dashed–dotted line) and FeNi (fcc, dashed line) alloys.

Analysis of the MAE of different types of over-layers, for instance of Co on Au(111) [76], Fe on Au(001) [77], and Co on Cu(001) [78]gives additional valuable information. For the case of Co on Au(111) [76] it was demonstrated that enhancement in the MAE could be understood from details in the DOS projected on the Co site, and in particular a large DOS at $E_{\rm F}$ with the 'correct' symmetry explained the large values of the MAE for certain thicknesses of an Au capping layer [76]. This way of explaining variations of the MAE was also reported by Pick and Dreyssé [79] who argued that a large MAE is expected when a large value of the DOS (of XY and YZ character) is situated on $E_{\rm F}$. Another important finding was also reported in Ref. [79], where the MAE of free standing mono–layers of Fe, Co and Ni was shown to have a minimum number of nodes as a function of band–filling.

9 Magneto–Striction

For strains close to the cubic phase, bcc and fcc, the change in the MAE is linearly dependent on the strain, ϵ (ϵ=c/a-1). Using arguments from magneto–elastic theory, the MAE of small tetragonal distortions can be used to calculate the magneto–striction coefficient, λ_{001}, as illustrated in Ref. [80] for fcc Ni. A similar scheme has been used by Wu et al. [81].The total energy can be written as the sum of an elastic and a magneto–elastic energy ($E_{\rm el}$ and $E_{\rm me}$) which are

assumed to be quadratic respectively linear in small distortions, $E_{\rm el}$ =Cϵ^2 and $E_{\rm me}$ =α B ϵ. Here ϵ is the volume conserving tetragonal distortion (ϵ˜ 2(c/a-1)/3), α is a constant which takes the value 1 for magnetization parallel to the tetragonal axis and -$\frac{1}{2}$ for a perpendicular direction, and B and C are the magneto–elastic and tetragonal elastic coefficients, respectively. The magneto–striction coefficient, λ_{001}, is defined as the equilibrium distortion, i.e. where the total energy, $E_{\rm el} + E_{\rm me}$, has its minimum, for the case with the magnetization along the [001] direction. By differentiation of the total energy with respect to ϵ this turns out to be $\lambda = -\frac{B}{2C}$. The uniaxial MAE is, for small distortions, related to the magneto–elastic energy as, $E_{\rm MAE} = \frac{3}{2}B\epsilon = 3\epsilon C\lambda$. Hence one may connect the λ and MAE values and compare their trends directly [32]. Hence, in order to study trends in the MAE as a function of, for instance, alloy concentration one may, as an alternative, study experimental trends in λ or the trend in the OMA, and this is something we will do next [32]. Before entering the details of such a comparison we comment that a rigid band approximation works well for studying the trends in the MAE and OMA of alloys involving Fe, Co and Ni [32]. In Fig. 12 we compare the calculated OMA of bcc Fe and fcc Co to the corresponding experimental magneto–striction coefficients, λ. All analyses [32] indicate that it is sensible to compare these two properties, at least their trends. Note that the theoretical calculations reproduce the experimental trends very well. For the FeCo alloy (bcc) theory reproduces the drop in λ with increasing Co concentration and the dip at a Co concentration corresponding to ˜2.5 spin down d–electrons. The trends in λ of the FeNi (fcc) alloys is somewhat more intricate where λ changes sign two times as a function of alloy concentration. However, theory and experiment agree rather well and we conclude that magneto–striction is a property which, at least concerning the trend, is accessible for state of the art, total energy calculations [32].

10 Summary

To summarize, we have outlined some of the most central aspects of first principles calculations of the magneto–crystalline anisotropy, and the spin and orbital moments of elements, compounds, interface and surface systems. One of the more commonly used methods for solving the Kohn–Sham equations, the full–potential linear muffin–tin orbital method is also reviewed, briefly. We give several examples of the accuracy of theory for reproducing the MAE, the spin and orbital moments, and the magneto–striction coefficients. A more detailed discussion of these effects can however be found in Ref. [63]. The most important results reviewed here is that the anisotropy of the orbital moment very often is connected to the MAE and the orbital moment may be influenced by a 'suitable' tuning of the electronic structure, via geometry, ligand atoms, crystal field splitting and so on. A theoretical engineering of suitable magnetic properties, such as magnitude of the moment and its directional behavior is now starting to become feasible. By good knowledge of how the electronic structure, and especially the

DOS projected on a specific atom type, is modified for different crystallographic environments, it is possible to predict materials with novel magnetic properties.

Acknowledgment

The support from the Swedish Natural Science Foundation is acknowledged. The support from the TMR is also acknowledged. Many of the results presented here are the result of a collaboration with O.Hjortstam, P.James, B. Johansson, L.Nordström, P.Ravindran, P.Söderlind and J.Trygg. We would like to thank the listed persons for this fruitful collaboration.

References

1. L.Nordström and D.Singh, Phys. Rev. Lett. **76**, 4420 (1996).
2. A.Aharoni, *Introduction to the Theory of Ferromagnetism*, (Oxford Science Publications, Oxford, 1998).
3. P.Bruno, Phys. Rev. B **39**, 865 (1989).
4. P.Hohenberg and W.Kohn, Phys. Rev. B**136**, 864 (1964).
5. W.Kohn and L.Sham, Phys. Rev. A **140**, 1133 (1965).
6. R.M.Dreitzler and E.K.U.Gross *Density Functional theory* (springer, berlin, 1990).
7. H.Eschrig, *The Fundamentals of Density Functional Theory* (Stutgart;Teubner, 1996).
8. R.Jones and O.Gunnarsson, Rev. Mod. Phys. **61**, 689 (1989).
9. J.Callaway and N.M.March, Rev. Mod. Phys. **38**, 689 (1989).
10. O.K.Andersen, Phys. Rev. B **12**, 3060 (1975).
11. H.L.Skriver, *The LMTO Method* (Springer verlag, Berlin, 1984).
12. I.Turek, V.Drchal, J.Kudrnovsky, M.Sob and P.Weinberger, *Electronic Structure of Disordered Alloys, Surfaces and Interfaces* (Kluwer Academic Publishers, Boston, 1997).
13. J.C.Slater, *The Self–Sonsistent Field of Molecules and Solids* (McGraw-Hill, New York, 1974).
14. T. L. Loucks, *Augmented Plane Wave Method* (W. A. Benjamin, Inc., New York, 1967).
15. D.J.Singh, *Planewaves, Pseudopotentials and the LAPW Method* (Kluwer Academic Publishers, Boston, 1994).
16. P.W.Atkins, *Molecular Quantum Mechanics*, Oxford University Press, Oxford, (1983).
17. H.Eschrig, *LCAO Method and the Electronic Structure of Extended Systems*, Springer-Verlag, Berlin (1989).
18. W.Harrison, *Electronic Structure and the Properties of Solids,* W.H.Freeman and Company, San Fransisco, 1980.
19. V.L.Morruzi, J.F.Janak, and A.R.Williams, *Calculated Electronic Properties of Metals* (Pergmon,New York,1978)
20. V.L.Morruzzis and C.B.Sommers, *Calculated Electronic Properties of Ordered Alloys, A Handbook* (World Scientific, Singapore, 1995).
21. L.H.Thomas, Proc.Cambridge Phil. Soc. **23**, 542 (1927); E.Fermi, Rend. Accad. Naz.Linzei **6**, 602 (1927).
22. Gell-Mann and K.A.Brueckner, Phys. Rev. **106**, 369 (1957).

23. E.P.Wiegner, Phys. Rev. 46, 1002, (1934).
24. D.M.Ceperly and B.J.Alder, Phys. Rev. Lett. **45**, 566 (1980)
25. G.P. Srivastava, J.Phys. A **17**, L317 (1984); O.Eriksson, J.Trygg, O.Hjortstam, B.Johansson and J.M.Wills, Surface Science **382**, 93 (1997).
26. N.W.Ashcroft and N.D.Mermin, *Solid State Physics* (Holt-Saunders Japan LTD.,1976)
27. O.Hjortstam (unpublished).
28. O.Jepsen and O.K.Andersen, Solid State Commun. **9**, 1763 (1971).
29. P.E.Blöchl, O.Jepsen, and O.K.Andersen, Phys. Rev. B **49**, 16223 (1994).
30. M.Methfessel and T.Paxton, Phys. Rev. B **40**, 3616 (1989).
31. O.Hjortstam, L.Nordström, B.Johansson, J.M.Wills, P.James and O.Eriksson (to be published).
32. P.James, L.Nordstrom, B.Johansson and O.Eriksson (to be published).
33. J.M.Wills (unpublished).
34. O.K.Andersen, First chapter in this book.
35. J.M.Wills, O.Eriksson, M.Alouani, and D.L. Price, Chapter 4 in this book.
36. J.H.van Vleck, Phys. Rev. B **52**, 1178 (1937).
37. H.Brooks, Phys. Rev. B **58**, 909 (1940).
38. E.I.Kondorski and E.Straub, Zh. Eksp. Teor. Fiz. **63**, 356 (1972).
39. B.R.A.Nijboer and F.W.De Wette, Physica (Amsterdam) **23**, 309 (1957); F.S.Ham and B.Segall, Phys. Rev. B **124**, 1786 (1961); B.R.A.Nijboer and F.W.De Wette, Physica (Amsterdam) **24**, 422 (1958).
40. G.H.O.Daalderop, P.J.Kelly and M.F.H.Schuurmans, Phys. Rev. B **41**, 11919 (1990).
41. M.S.S.Brooks and P.J.Kelly, Phys. Rev. Lett. **51**, 1708 (1983).
42. D.D.Koelling and B.N.Harmon, J.Phys. C **10**, 3107 (1977).
43. M.E.Rose, *Relativistic Electron Theory*, (John Wiley and Sons. New York, 1961).
44. O.Eriksson, Thesis (Uppsala University).
45. C.Li, A.J.Freeman, H.J.F.Jansen, and C.L.Fu, Phys. Rev. B **42**, 869 (1990).
46. J.C.Bradley and A.P.Cracknell, *The Mathematical Theory of Symmetry in Solids*, Clarendon Press, Oxford, 1972.
47. O.Eriksson, M.S.S.Brooks and B.Johansson, Phys. Rev.B **41**, 7311(1990).
48. G.Racah, Phys. Rev. **61**, 186 (1949).
49. J.K.Jorgensen, *Electrons in Atoms and Molecules* (Academic Press, London, 1962).
50. J.H.van Vleck, Phys. Rev. **45**, 405 (1934).
51. C.J.Ballhausen, *Crystal Field Theory*, McGraw-Hill, New York, 1962.
52. M.Norman, Phys. Rev. Lett. **64**, 1162 (1990).
53. L.J.Nuget, J.Inorg. Nucl. Chem. **32**, 3485 (1970).
54. L.Severin, M.S.S.Brooks, and B.Johansson, Phys. Rev. Lett. **71**, 3214 (1993).
55. P.Söderlind, O.Eriksson, R.C.Albers., A.M.Boring, and B.Johansson, Phys. Rev. B **45**, 12911 (1992).
56. O.Eriksson, B.Johansson, R.C.Albers, A.M.Boring, M.S.S.Brooks, Phys. Rev. B **42**, 2707 (1990).
57. H.Ebert et al.,J.Appl. Phys. **67**, 4576 (1990).
58. J.Trygg, B.Johansson, O.Eriksson and J.M.Wills, Phys. Rev. Lett.**75**, 2871 (1995).
59. T.Suzuki (unpublished).
60. S.V.Halilov, A.Ya.Perlov,P.M.Oppeneer,.A.N.Yaresko and V.N.Antonov, Phys. Rev. B **57**, 9557 (1998).
61. O.K.Andersen, H.L.Skriver, H.Nohl, and B.Johnasson, Pure and Appl. Chem. **52**, 93 (1980).

62. X.Wang, D.-S.Wang, R.Wu and A.J.Freeman, J.M.M.M. **159**, 337 (1996).
63. P.James, Thesis (in print).
64. O.Hjortstam, K.Baberschke, J.M.Wills, B.Johansson, and O.Eriksson, Phys. Rev. B **55**, 15026 (1997).
65. S.Muller, B.Schulz, G.Kostka, M-Fahrle, K.Heinz, and K.Baberschke, Surf. Sci. **364**, 235 (1996).
66. O.Heckmann, H.Magnan, P.le Fevre, D.Chanderis, and J.J.Rehr, Surf. Sci. **312**, 62 (1994).
67. B.Schulz, K.-Baberschke, Phys. Rev. B **50**, 13467 (1994); K.Baberschke, Appl. Phys. A **62**, 417 (1996).
68. U.Gradman, Ann. Phys. (N.Y.) **17,** 91 (1966).
69. P.Ravindran, P.James, J.M.Wills and O.Eriksson (unpublished).
70. G.H.O.Daalderop, P.J.Kelly, M.F.H.Schuurmans, Phys. rev. B **42**, 7270 (1990).
71. M.Tischer, O.Hjortstam, D.Arvanitis, J.Hunter Dunn, F.May, K.Baberschke, J.Trygg, J.M.Wills, B.Johansson and O.Eriksson, Phys. Rev. Lett. **75**, 1602 (1995).
72. enhancement of ni spin moment at surface
73. B.T.Tole, et al. Phys. Rev. Lett. **68**, 1943 (1992); P.Carra et al. Phys. Rev. Lett. **70**, 694 (1993).
74. O.Hjortstam, J.Trygg, J.M.Wills, B.Johansson and O.Eriksson, Phys. Rev B **53**, 9204 (1996).
75. O.Eriksson, et al. Solid State Commun.**78**, 801 (1991); O.Eriksson, et al. Phys. Rev. B **45**, 2868 (1992).
76. B.Ujfalussy, L.Szunyogh, P.Bruno, and P.Weinberger, Phys. Rev. Lett. **77**, 1805 (1996).
77. L.Szunyogh, B.Ujfalussy and P.Weinberger, Phys., Rev. B **51**, 9552 (1995).
78. L.Szunyogh, B.Ujfalussy,U.Pustogowa, and P.Weinberger, Phys. Rev. B **57**, 8838 (1998).
79. S.Pick and H.Dreysse, Phys. Rev. B **46**, 5802 (1992).
80. P.James et al (unpublished)
81. R.Wu et al. (unpublished).